Far from home: a multi-analytical approach revealing the journey of an African-born individual to imperial Rome

Kevin Salesse[a,b], Élise Dufour[c], Vincent Balter[d], Robert H. Tykot[e], Nina Maaranen[f], Maïté Rivollat[b,g], Arwa Kharobi[b,f], Marie-France Deguilloux[b], Marie-Hélène Pemonge[b], Jaroslav Brůžek[b,h], Dominique Castex[b]

[a]Unit of Anthropology and Human Genetics, Université Libre de Bruxelles, Campus du Solbosch, CP192, Avenue F.D. Roosevelt 50, 1050 Brussels, Belgium; [b]PACEA - De la Préhistoire à l'Actuel: Culture, Environnement et Anthropologie, UMR 5199, Université de Bordeaux, CNRS, Bâtiment B8, allée Geoffroy Saint Hilaire, CS50023, 33615 Pessac cedex, France; [c]Archéozoologie, Archéobotanique: Sociétés, Pratiques et Environnements, AASPE UMR 7209, Muséum national d'Histoire naturelle, CNRS, CP55, 55 rue Buffon, 75005 Paris, France; [d]Laboratoire de Géologie de Lyon: Terre, Planète, Environnement, UMR 5276 (CNRS, ENS, Université Lyon1), École Normale Supérieure de Lyon, 69364 Lyon cedex 07, France; [e]Department of Anthropology, University of South Florida, 4202 East Fowler Avenue, SOC107, Tampa, FL 33620, USA; [f]Department of Archaeology and Anthropology, Bournemouth University, Talbot Campus, Poole BH12 5BB, United Kingdom; [g]Department of Archaeogenetics, Max Planck Institute for Science of Human History, Kahlaische Strasse 10, 07745 Jena, Germany; [h]Department of Anthropology and Human Genetics, Faculty of Science, Charles University, Viničná 7, 12844 Praha 2, Czech Republic.

Email Addresses: Kevin Salesse (Kevin.Salesse@ulb.be); Élise Dufour (elise.dufour@mnhn.fr); Vincent Balter (vincent.balter@ens-lyon.fr); Robert H. Tykot (rtykot@usf.edu); Nina Maaranen (nmaaranen@bournemouth.ac.uk); Maïté Rivollat (maite.rivollat@u-bordeaux.fr); Arwa Kharobi (akharobi@bournemouth.ac.uk) ; Marie-France Deguilloux (marie-France.deguilloux@u-bordeaux.fr) ; Marie-Hélène Pemonge (marie-helene.pemonge@u-bordeaux.fr); Jaroslav Brůžek (Yaro@seznam.cz); Dominique Castex (dominique.castex@u-bordeaux.fr).

Corresponding Author: Kevin Salesse (Kevin.Salesse@ulb.be); Unit of Anthropology and Human Genetics, Université Libre de Bruxelles, Campus du Solbosch, CP192, Avenue F.D. Roosevelt 50, 1050 Brussels, Belgium. ORCID number: 0000-0003-2492-1536

Formatted: English (United States)

ABSTRACT

Rome saw its number of foreign individuals increase considerably as the empire expanded. These foreigners arrived as either free persons or slaves from the newly conquered provinces and near-frontier zones and came to influence the whole life of the city. Yet relatively little is known about their life histories. In this study, we bring direct evidence for the first example of an African-born migrant, with an origin beyond the southern imperial border, discovered in Rome. Based on a multi-tissue sampling strategy including molar teeth and mandibular cortical bone, a multi-analytical approach including isotopic ($\delta^{13}C$, $\delta^{15}N$, $\delta^{18}O$, $\delta^{34}S$, $^{87}Sr/^{86}Sr$), dental morphology (geometric morphometrics, nonmetric traits) and ancient DNA (mitochondrial DNA, Y chromosome) analyses allows reconstructing the journey and lifeway patterns of the individual US215/Mand1 buried in the mass grave from the catacombs of Saints Peter and Marcellinus. The successful isotopic and dental morphology analyses suggest that the individual was probably born in the vicinity of the Nile Valley or within the central Sahara Desert. Results also suggest a diachronic change of residence in the area during their early life. The way US215/Mand1 reached Rome is still hypothetical, although it seems likely that the individual could have undergone forced migration as a slave to the capital.

Keywords: Stable and radiogenic isotopes, dental morphology, ancient DNA, mobility, diet, Roman period

1. INTRODUCTION

During the last centuries of the Republic and the early ones of the Empire, foreign populations of Rome increased very swiftly and, in many ways, came to influence the whole life of the city. Individuals from the newly conquered provinces and from the near-frontier zones reached the Imperial capital, and a large part of them arrived as enslaved individuals (Abrecht, 2019; de Ligt and Tacoma, 2016; La Piana, 1927; Noy, 2000; Tacoma, 2016). Trans-Saharan slave trade and slave traffic across the southern Egyptian border are well-attested during the 1st-3rd century AD, although little evidence is available regarding the scale and the intensity of these imports (Kirwan, 1957; Law, 2009; Snowden Jr., 1947; Wilson, 2012). Ascertaining the number of North African-born slaves and their descendants among the Rome's population is almost impossible, despite the low number often suggested (George, 2003; Tacoma, 2012). Dark-skinned or black Africans were surely a minority among the slave workforce, the majority of which originated from northernmost and easternmost regions of the Roman world (George, 2003; Gordon, 1924; Wilson, 2012). Also, the trade of enslaved Africans remained a limited fraction of the Empire's total slave supply (Wilson, 2012). In Roman times, Africans who originated from outside the Empire, like all other slaves, may have gained wealth and autonomy as well as achieve a degree of social status (George, 2003). Romans were fond of exoticism, and the ownership of rare slaves signaled prominent social rank (George, 2003; McLaughlin, 2014). Removed from the geographical confines of their original home, African-born slaves were exploited in the domestic households of the Roman elite. By exhibiting the possession of such slaves, a slave-owner could display a level of sophistication among their *familia* as well as exhibit their wealth and worldliness (George, 2003). However, African slaves could also have served in Rome's armed forces or worked for public institutionsor temples (Lenski, 2006; Silver, 2016; Weiss, 2004). Immigration of free men and women must not have been very large in comparison with the importation of slaves. The city of Rome could not attract a large number of foreign workers since most industries already used a servile population. However, the imperial Rome always had a few wholesale merchants, shipowners, bankers, retail traders or adventurers, in pursuit of success, and among them were many foreigners (Abrecht, 2019; de Ligt and Tacoma, 2016; La Piana, 1927; McLaughlin, 2014). Nevertheless, there is, to the best of our knowledge, little indications of such individuals born beyond the southern imperial frontier and established in the capital.

The catacombs of Saints Peter and Marcellinus (hereafter: the SSPM catacombs), located at the third milestone of the ancient Via Labicana, near the modern via Casilina in the south-east of Rome (WGS 84: 41°52'43.4"N 12°32'54.6"E; Precision: exact) is a unique example to further discuss this topic. Among our recent bioarcheological investigations of the SSPM assemblage, one individual, labeled

US215/Mand1, drew our attention. Their initial stable oxygen isotope values ($\delta^{18}O_{sc\ (enamel)}$ up to +2.7‰ – see Results) were very atypical for Rome and suggested a non-European origin, possibly African. To refine the life history (dietary patterns, mobility, geographical origin, and ancestry) of this individual in their population, social and geopolitical contexts, a multi-analytical approach using additional isotopic measurements on both bone and tooth ($\delta^{13}C$, $\delta^{15}N$, $\delta^{18}O$, $\delta^{34}S$, $^{87}Sr/^{86}Sr$), dental morphology analyses (geometric morphometrics, nonmetric traits) and ancient DNA investigation (mitochondrial DNA, Y chromosome) have been performed and presented here.

2. THE CATACOMBS OF SAINTS PETER AND MARCELLINUS

In the early 2000s, several mass graves containing circa 3,000 skeletons were fortuitously discovered in the oldest part of the SSPM catacombs (i.e. Region X), near the sanctuary of the eponymous saints (Blanchard et al., 2007; Giuliani et al., 2007). The discovered area is characterized by the presence of seven interconnected cavities of various shapes, dimensions and elevations (Fig. 1), and distinct from the other burial chambers (i.e. *cubiculum*) or crypts commonly found in catacomb systems (Blanchard et al., 2007). Archaeological excavations conducted from 2004 to 2010 have made it possible to document the main characteristics of skeletal accumulations and to suspect their relationship with one or more mortality crises (Castex et al., 2007, 2009, 2011). Skeletons were found articulated and placed next to each other or in piles. The new corpses were deposited without disturbing the old ones, and no filling was accumulated among individuals buried in the same level. This evidence in conjunction with the relationship between the capacity of the burial chambers and the volume of the bodies as well as the taphonomic evolution of all the layers of corpses together suggested that several successive multiple inhumations were carried out (Castex et al., 2014; Kacki et al., 2014). The very low frequency (< 5%) of traumatic lesions on the assemblage excludes the hypothesis of interpersonal violence as the cause of death (e.g. massacres, martyrdom or human sacrifice) (Castex and Blanchard, 2011). Altogether, the data argue for mortality events of epidemic origin, occurring over a relatively short timeframe (Castex and Blanchard, 2011; Castex et al., 2014). A significant number of the individuals were given highly elaborate funerary practices, never previously recorded in Rome, including the use of gypsum-plastered textiles as body wrappings together with precious and exotic foreign resinous substances (i.e. succinite, sandarac and frankincense) (Devièse et al., 2017; Schotsmans et al., 2019). The high-level care offered to the deceased as well as the presence of good-to-high quality textile remains (e.g. gold and probable silk threads, fineness of the weave) suggested that at least part of these individuals belonged to the upper classes of the Roman society (Blanchard et al. 2015; Devièse et al., 2017). Analysis of grave goods and ^{14}C data revealed that the

mass graves dated back to the early imperial period (1st-3rd c. AD) (Blanchard et al., 2015; Castex and Blanchard, 2011).

3. MATERIAL

The individual US215/Mand1 was found in the chamber X83 during a rescue survey conducted prior to the construction of a support pillar to secure the site (Fig. 2). Time limitation as well as structural instability constrained investigators to remove human remains rapidly in layers of 20 centimeters in thickness at this location. In the prospect of a large-scale isotopic study in the SSPM catacombs, a minimum number of individuals of 14 based on right hemi-mandibles with at least the second molar embedded was estimated on this assemblage (Salesse 2015). Among them was US215/Mand1, represented by only three lower right permanent molars in the mandible fragment (Fig. 3).

Enamel of all teeth as well as a piece of mandibular cortical bone were sampled to isotopically investigate diet and mobility of US215/Mand1. This multi-tissue sampling strategy allows exploiting the differential growth timing of skeletal elements in order to reconstruct a detailed life history, at the scale of the individual (see Supplementary File A). The isotopic results from US215/Mand1 have been compared to those of the rest of the corpus (n = 129 individuals) from the Region X mass graves (Salesse 2015) and then have been geographically recontextualized by comparisons with animal and human populations from Italy or beyond (Buzon and Simonetti, 2013; di Lernia et al., 2013; Killgrove and Tykot, 2013, 2018; Nitsch, 2012; O'Connell et al., 2019; Prowse et al., 2004; Rutgers et al., 2009; Schrader et al., 2019; Sereno et al., 2008; Stojanowski and Knudson, 2011, 2014; Tafuri et al., 2006, 2018).

A small dataset (right-side mandible fragments with molars) from the mass graves of the catacombs (n = 13, including US215/Mand1; Table 1), available at the time of this study, have been used to explore biodistance through dental nonmetric traits. Further exploration of molar outline shape was conducted on US215/Mand1 and a subset of individuals from the SSPM catacombs (n = 4, Table 1) using geometric morphometrics.

Dentine of the US215/Mand1's second molar has been sampled for exploring the paternal and maternal lineages through ancient DNA analysis. Teeth of a small batch of individuals (n = 5, Table 1) randomly selected in the mass graves of the catacombs have also been investigated for comparative purposes.

4. METHODS

The principles of the stable isotope analysis (including abbreviations), the dental morphology study and the paleogenetic approach are set out in Supplementary File A.

4.1. Isotopic analysis

4.1.1. Bone collagen extraction for $\delta^{13}C$, $\delta^{15}N$, and $\delta^{34}S$ analyses

Bone preparation and chemical pretreatments were conducted at the stable isotope preparation lab of UMR 7209 in the *Muséum National d'Histoire Naturelle* (MNHN) (Paris, France). Sampled bones were cleaned using a tungsten carbide drill bit to retain only compact parts. Bone collagen was extracted following the protocol of Longin (1971), modified by Bocherens et al. (1988, 1991). Bones were crushed using a knife mill or a mortar and pestle. Powder samples (amount: ≃ 400 mg; grain size: 0.3 to 0.7 mm) were decalcified in 40 ml of 1 M hydrochloric acid (HCl) at room temperature for 20 min. Gelatins were retrieved by filtration using a MF-Millipore membrane filter (pore size: 5 µm), rinsed, and then soaked into 0.125 M sodium hydroxide at room temperature for 20 h to remove soil organic matter. The samples were again filtered and rinsed. Gelatins were solubilized in 0.01 M HCl (pH = 10^{-2}) at 100° C for 17 h and filtered a last time to trap possible impurities. Collagen samples were freeze-dried at -87° C for at least 48 h and extraction yields (%Col) were calculated (expressed as a weight percentage, wt.%). In modern bones, extraction yields are around 20.4 ± 3.9 wt.% (1SD) (Bocherens et al., 1991), and samples containing less than 1 wt.% of collagen are considered unreliable (Dobberstein et al., 2009; Van Klinken, 1999).

Carbon and nitrogen abundances and isotope compositions were measured (amount: 200-400 µg) using a Costech Elemental Analyzer 4010 fitted with a zero-blank auto-sampler coupled via a ConFlo IV to a ThermoScientific Delta V PLUS Isotope Ratio Mass Spectrometer at the environmental isotope laboratory of the James Cook University's advanced analytical center (Cairns, Australia). Carbon and nitrogen contents are expressed as percentages (%C and %N). In modern bones, %C and %N values range from 15.3 to 47% and from 5.5 to 17.3%, respectively (Ambrose, 1990). Samples with %C and %N values below 13% and 4.8%, respectively, are recognized as severely altered (Ambrose, 1990; Garvie-Lok, 2001; Iacumin et al., 1998; Reitsema, 2012; Van Klinken, 1999). Atomic C:N ratios of modern bones vary between 2.9 and 3.6 (DeNiro, 1985), and archaeological samples with values below or above these thresholds indicate alteration or contamination. The $\delta^{13}C_{col}$ and $\delta^{15}N_{col}$ values are reported as per mil (‰) difference relative to VPDB and AIR, respectively. International and in-house standards (USGS-40: $\delta^{13}C$ = -26.4‰ and $\delta^{15}N$ = -4.5‰; Taipan: $\delta^{13}C$ = -11.7‰ and $\delta^{15}N$ = 11.8‰; Chitin: $\delta^{13}C$ = -19‰ and $\delta^{15}N$ = 2.2‰) were analyzed for quality control. During this study, analytical errors

calculated from replicates of internal standards were better than ± 5% (1SD) for both %C and %N, ± 0.1‰ (1SD) for $\delta^{13}C_{col}$ and ± 0.2‰ (1SD) for $\delta^{15}N_{col}$.

Sulfur abundance and isotope composition were assessed (amount: 7-8 mg) using a Costech Elemental Analyzer 4010 coupled with a ThermoScientific Delta V Advantage isotope ratio mass spectrometer at the University of South Florida Stable Isotope Lab (Tampa, Florida, USA). Sulfur content is expressed in percentages (%S). In modern bones, %S values as well as the atomic C:S and N:S ratios range from 0.15 to 0.35%, from 300 to 900, and from 100 to 300, respectively (Bocherens et al., 2011; Nehlich and Richards, 2009). Bone collagen samples with values outside these ranges are considered unreliable. The $\delta^{34}S$ results are reported as per mil (‰) deviation and normalized to CDT using certified and in-house reference materials (IAEA-S2: $\delta^{34}S$ = 22.7‰; IAEA-S3: $\delta^{34}S$ = -32.3‰; and Elemental Microanalysis B2155: $\delta^{34}S$ = 6.7‰). Measurements errors calculated from 46 replicates of the B2155 standard were ± 0.11% (1SD) for %S and ± 0.36‰ (1SD) for $\delta^{34}S_{col}$.

4.1.2. Bone and tooth carbonate preparation for $\delta^{13}C$ and $\delta^{18}O$ analyses

Bone carbonate preservation was investigated by Fourier transform infrared (FTIR) spectroscopy in attenuated total reflection (ATR) mode before pretreatments (see Lebon et al. 2011 and Salesse et al. 2014 for a presentation of the protocol used). The diagenetic trajectory of bone samples from the SSPM catacombs has already been described in Salesse et al. (2014).

Bone and tooth carbonate samples were prepared following a revised version of the protocol of Balasse et al. (2002) at the MNHN. Sampled bones were crushed as described above. Selected teeth were first cleaned and then sampled over the entire height of the crown with a tungsten carbide drill bit. Powder samples (amount: ≃ 30 mg; grain size < 0.3 mm) were treated with 1.5 ml of 2-3% sodium hypochlorite (NaClO) at room temperature for 48 h to remove organic matter, and then with 1.5 ml of 1 M acetic acid (CH_3COOH) at room temperature for 1 h to remove exogenous carbonates. NaClO and CH_3COOH solutions were renewed at least once during the procedure. Samples were rinsed with distilled water between the two steps and at the end. Samples were oven-dried at 65° C overnight. The purification process induced significant weight losses, up to 80%.

Carbon and oxygen isotope compositions were measured (amount: 580-630 µg) via a ThermoScientific Kiel IV carbonate device interfaced with a ThermoScientific Delta V Advantage isotope ratio mass spectrometer at the MNHN's isotope-ratio mass spectrometry service. The results are reported as per mil (‰) deviation from VPDB reference standard scale. An in-house carbonate standard (Marble LM: $\delta^{13}C$ = 2.13‰ and $\delta^{18}O$ = -1.83‰), normalized to the international standard NBS 19, was used for checking the accuracy of the measurements. Analytical precision calculated from 107 replicates of Marble LM were ± 0.03‰ (1SD) for $\delta^{13}C$ and ± 0.07‰ (1SD) for $\delta^{18}O$.

240
241 *4.1.3. Tooth enamel sample preparation for $^{87}Sr/^{86}Sr$ analysis*
242
243 Samples were processed in a clean room with filtered air and under laminar-flow hoods at the
244 *École Normale Supérieure* (ENS) (Lyon, France). Enamel samples were prepared as mentioned above.
245 Powder samples (amount: ≃ 30 mg; grain size < 0.3 mm) were ultrasonicated in 1 ml of 0.1 M CH_3COOH
246 for 5 min to eliminate diagenetic carbonates, rinsed with MilliQ water to neutral, and then freeze-dried
247 at -50° C for at least 12 h. Samples were then dissolved in 1 ml of 4 M of nitric acid (HNO_3). An aliquot
248 of 100 µl was taken from each sample for trace element concentration analysis.
249 Strontium was isolated following a similar protocol to that described in De Muynck et al. (2009).
250 Teflon ion exchange columns were filled with 2 ml of 50-100 µm bead size TrisKem Sr-Resin. Resin was
251 washed with MilliQ water and 0.05 M HNO_3, and then pre-conditioned with 3 ml of 4 M HNO_3. The
252 dissolved samples were loaded into the columns. Column blanks were prepared with 1 ml of 4 M HNO_3.
253 Columns with samples were rinsed with 5 ml of 4 M HNO_3 to remove concomitant matrix elements,
254 and then with 6 ml of 0.05 M HNO_3 to strip off the purified strontium fraction. Retrieved strontium
255 samples were evaporated, and dried residues were finally dissolved in 1 ml of 0.05 M HNO_3.
256 Strontium concentrations were determined using an Agilent 7500 CX inductively coupled plasma
257 mass spectrometry following the method of Balter and Lécuyer (2010), whereas strontium isotope
258 ratios were measured using a large-radius Nu 1700 multi-collector inductively coupled plasma mass
259 spectrometer, both at the ENS. Strontium isotope data were obtained at low-resolution in static mode.
260 Signal intensities were monitored on ^{83}Kr and ^{85}Rb and used to correct for interferences on *m/z* ratios
261 of 84 (Kr), 86 (Kr), and 87 (Rb). Ratios were corrected for mass bias fractionation using an internal
262 normalization to $^{86}Sr/^{88}Sr = 0.1194$. Gas flow instrumental mass fractionation was controlled with a
263 standard-sample bracketing approach involving the measurement of the standard NIST SRM 987
264 (recommended value of $^{87}Sr/^{86}Sr = 0.710248$; McArthur et al., 2001). Samples were randomized during
265 analysis and duplicates were measured to check for systematic errors. Repeated measurements of
266 NIST SRM 987 standard yielded an average value of $^{87}Sr/^{86}Sr = 0.71025 \pm 0.00002$ (2SD; 12 analyses).
267
268 *4.1.4. Isotopic data processing*
269
270 The Bayesian model FRUITS (Food Reconstruction Using Isotopic Transferred Signals, version 2.1.1;
271 Fernandes et al. 2014) was applied to evaluate the relative importance of plant and animal resources
272 in the US215/Mand1's diet as well as estimate their protein and carbohydrate/fat intakes. The model
273 parameters used are detailed in the Supplementary File B.

To reconstruct the $\delta^{18}O_{dw\ (enamel)}$ values of US215/Mand1, three steps were followed: 1) converting $\delta^{18}O_{sc\ [VPDB]}$ into $\delta^{18}O_{sc\ [VSMOW]}$ values using the equation of Coplen (1988) (Eq. 1); 2) estimating $\delta^{18}O\text{-}_{phosphate\ [VSMOW]}$ from $\delta^{18}O_{sc\ [VSMOW]}$ values via the equation developed by Chenery et al. (2012) (Eq. 2); and 3) calculating $\delta^{18}O_{dw\ [VSMOW]}$ from $\delta^{18}O_{phosphate\ [VSMOW]}$ values thanks to the formula proposed by Daux et al. (2008) (Eq. 3).

Equation 1. $[\delta^{18}O_{sc\ [VSMOW]} = 1.03091 \times \delta^{18}O_{sc\ [VPDB]} + 30.91]$

Equation 2. $[\delta^{18}O_{phosphate\ [VSMOW]} = 1.122 \times \delta^{18}O_{sc\ [VSMOW]} - 13.73]$

Equation 3. $[\delta^{18}O_{dw\ [VSMOW]} = 1.54 \times \delta^{18}O_{phosphate\ [VSMOW]} - 33.72]$

To reconstruct the $\delta^{18}O_{dw\ (bone)}$ values of US215/Mand1, two steps were followed: 1) converting $\delta^{18}O_{sc\ [VPDB]}$ into $\delta^{18}O_{sc\ [VSMOW]}$ values using the equation of Coplen (1988) (Eq. 1); and 2) calculating $\delta^{18}O_{dw\ [VSMOW]}$ from $\delta^{18}O_{sc\ [VSMOW]}$ via the equation proposed by Chenery et al. (2012) (Eq. 4).

Equation 4. $[\delta^{18}O_{dw\ [VSMOW]} = 1{,}59 \times \delta^{18}O_{sc\ [VSMOW]} - 48{,}634]$.

These two procedures are recommended by Chenery et al. (2012) for individuals originating from geographical regions characterized by a hot-arid climate and for individuals originating from the rest of the world, respectively.

Finally, all the isotopic data, together with associated chronological and other supporting information, from this study have been uploaded in the IsoArcH database (Salesse et al., 2018, 2020).

4.2. Dental morphology analysis

4.2.1. Nonmetric traits

Dental traits (see list in Table 2) were recorded either as present/absent or as a grade from absent to full expression, following the appropriate guidelines (i.e. Marado and Silva, 2016; Pilloud et al., 2018; Scott and Irish, 2017). An interesting dental nonmetric trait, crenulation, was included in the investigation. The trait is currently not part of the ASUDAS but has recently been explored further by Pilloud et al. (2018) who observed highest frequencies (and scores) for the trait among modern American Black and South African samples.

As recommended, each trait was represented by one tooth in the final analysis to prevent redundancy (Irish, 2005; Nichol, 1990). To analyze the dental nonmetric data, a distance matrix was created using Gower distances which measures the distance between pairs and then combines the distances into a single value per record-pair (Gower, 1971). This allows for missing data and the use of a mixed dataset of interval, ordinal and categorical data. However, the generated distance matrix is non-Euclidean, requiring nonparametric tools for further data analysis. The distance matrix was created using the function daisy in R package cluster (Maechler et al. 2019), allowing the user to define

symmetric and asymmetric binary values (e.g. in the case rare traits). The morphological similarities were further analyzed using the function pam in cluster, which partitions the data into clusters around medoids represented by individual datapoints. Data was visualized using nonmetric multidimensional scaling (NMDS) and t-distributed Stochastic Neighbor Embedding (t-SNE). Both are dimension reduction techniques intended to condense data to a visually observable form. The former is a built-in statistical tool in R (R Core Team, 2020), the latter was created using the R package Rtsne (van der Maaten and Hinton, 2008).

4.2.2. Geometric morphometrics

Geometric morphometrics was utilized to explore shape change between a subset of individuals, with the individual of interest as reference. To investigate only the shape of organism, size, location and orientation must be excluded from the coordinates. The most common method to do this is the generalized Procrustes superimposition where landmarks are rotated to best fit, centered and rescaled to a size 1 (Webster and Sheets, 2010). The coordinates exist in Kendall's shape space (Kendall, 1984), defined as a mathematical space induced by the shape coordinates (Mitteroecker and Gunz, 2009). To treat the semi-landmarks, bending energy (Bookstein, 1997) which maps the 'path of least resistance' between neighboring landmarks, was used.

The mandible fragments were digitized using the R package Stereomorph (Olsen and Westneat, 2015), which created shape files for each sample, and analyzed with the sibling package geomorph (Collyer and Adams, 2018). Due to attrition on the occlusal surfaces (and the subsequent loss of landmark information), the analysis was constricted to an investigation of the outline created by the three molars, using two landmarks as anchor and semi-landmarks to map the outline. The landmarks were used only momentarily, the analysis focusing on semi-landmark-based outline due to heavy wear, as Stereomorph requires them to create a start and end point for the semi-landmarks. To make sure the outline resembles the tooth shape as well as possible, the landmarks were placed at the meeting point of cusp 3 and 5 on LM1, as close to one another as possible, while the semi-landmarks were placed around the tooth in the same direction. Before connecting the semi-landmarks, they were redistributed around the shape in even distances using the package function lapply. Because we wanted to create a closed outline of the three molars, the landmarks were omitted from the outline and to avoid duplication of the points (landmarks would correlate with the first and last semi-landmark along the curve). Generalized Procrustes superimposition was then performed using function gpagen. The differences between individuals were visualized using functions plotTangentSpace, performing PCA, and plotRefToTarget which place the configuration on a grid and deforms it in locations where change is observed.

344

345 4.3. aDNA extraction and analysis

346

347 Ancient DNA (aDNA) analyses were not anticipated before the excavation. The teeth were
348 therefore decontaminated, i.e. scraped, cleaned with bleach, and subsequently exposed to UV
349 radiation for 20 min on each side. All established aDNA guidelines were then followed to minimize
350 contamination during subsequent steps. Analyses were conducted in the aDNA facilities of UMR PACEA
351 at Bordeaux University (Pessac, France). The teeth were powdered and a sample of 100 mg for each
352 was incubated overnight in lysis buffer (0.5 M EDTA, pH 8, 25 mg/ml proteinase K, and 0.5% N-Lauryl
353 sarkosyl). The procedure of Allentoft et al. 2015 was then followed to extract the DNA (MinElute kit,
354 Qiagen). In order to assess maternal (mitochondrial DNA) and paternal (Y chromosome) lineages, a
355 combination of 18 mitochondrial and 10 Y chromosome SNPs were typed through one multiplex using
356 MALDI-TOF MS-based SNP genotyping (iPLEXTM Gold technology, Sequenom, Inc., San Diego, CA,
357 USA). All primers used for these experiments and procedure details are available in Rivollat et al.
358 (2015). This first set of analyses was also designed to test for the ancient DNA conservation in the
359 human remain and, in case of sufficient DNA preservation, was supposed to be followed by the
360 characterization of the mitochondrial first hypervariable region (HVR-I, nps 16,024–16,380) targeted
361 using four overlapping fragments (following the procedures described in Rivollat et al., 2015).

362

363 5. **RESULTS**

364

365 5.1. Mobility and dietary patterns of US215/Mand1 through stable isotopic data

366

367 Collagen was successfully extracted from the mandibular fragment of US215/Mand1. With an
368 extraction yield of 6.7 wt.%, it exceeds the minimum threshold of 1 wt.% indicating a satisfactory
369 sample preservation (Table 3). With 38.5%, 13.6% and 0.31% respectively, carbon, nitrogen and sulfur
370 contents fall into the reference ranges for well-preserved collagen samples (Table 3). The atomic C:N,
371 C:S and N:S ratios are 3.3, 331.2 and 100.3 respectively, which is well within the acceptable ranges of
372 variation for unaltered and uncontaminated collagen samples (Table 3). Therefore, the collagen extract
373 of this individual meets all the criteria for good-quality collagen. Regarding the FTIR indicators for bone
374 carbonate preservation, the mandible fragment of US215/Mand1 presents an IRSF value of 4.1, a
375 CO_3/PO_4 ratio of 0.46 and an Amide I/PO_4 ratio of 0.24. These values differ significantly from those
376 measured on modern reference samples (see Salesse et al. 2014 and references therein). Compared
377 to the rest of the population (Salesse et al. 2014), US215/Mand1 falls into the group of bones

moderately recrystallized. It was, however, demonstrated that samples falling in this group had reliable carbonate isotope signals (Salesse et al. 2014). Tooth preservation was not investigated since it is widely recognized that enamel can survive most diagenetic regimes and preserve biogenic isotopic signals, especially in European archaeological contexts as young as the Roman ones (e.g. Koch et al., 1997; Wang and Cerling, 1994; Zazzo, 2014). The isotopic results obtained in this study can therefore be considered reliable and used to explore mobility and diet.

US215/Mand1 exhibits $^{87}Sr/^{86}Sr_{enamel}$ ratios of 0.7085, 0.7086 and 0.7087 for M1, M2 and M3, respectively (Table 4; Fig. 4). These $^{87}Sr/^{86}Sr_{enamel}$ ratios are within one standard deviation from both the SSPM and the other Lazio population means (Fig. 4 and 5). Further, US215/Mand1 presents $\delta^{18}O_{sc\ (enamel)}$ values of +1.3‰, +2.3‰ and +1.2‰ for M1, M2 and M3, respectively (Table 4). These $\delta^{18}O_{sc\ (enamel)}$ values are significantly much higher than the rest of the population from the region X of the SSPM catacombs (Grubb's tests; $p < 0.00$) (Fig. 4), and other Roman individuals from Lazio (Grubb's tests; $p < 0.00$) (Fig. 6). In contrast, with a $\delta^{18}O_{sc\ (bone)}$ value of -3.0‰ (Table 4), US215/Mand1 lies within one standard deviation from the population mean (Fig. 4). The estimated $\delta^{18}O_{dw}$ values of US215/Mand1 vary between +0.7‰ and +2.6‰ on teeth and it is +4.4‰ on bone (Table 4).

Breastfeeding and weaning could theoretically explain the high $\delta^{18}O_{sc\ (enamel)}$ values of US215/Mand1. Breast milk is enriched in ^{18}O over the consumed drinking water, inducing elevated $\delta^{18}O$ in infant tissues (Britton et al., 2015). Among modern humans living in non-industrialized and traditional fertility societies, cessation of breastfeeding occurs in most cases between the age of two or three (Alvarez, 2000; Britton et al., 2015; Kennedy, 2005; Sellen, 2001, 2007). Such a pattern was also identified in Roman populations over the Empire based on isotopic but also written evidence (for Rome, see Prowse et al., 2008; for Africa, see Dupras et al. 2001; Keenleyside et al. 2009). Among teeth, only permanent first molars have their crown mineralized between birth and the age of three; the other molars covering posterior age periods (Moorrees et al., 1963). Thus, breastfeeding processes affect commonly only isotopic signals of M1s. These effects are, however, relatively limited, and lead to an increase of $\delta^{18}O_{sc\ (enamel)}$ by approximately +0.7‰ (Herring et al., 1998; Knudson, 2009; Roberts et al., 1988; Wright and Schwarcz, 1998, 1999). US215/Mand1 has a lower $\delta^{18}O_{sc\ (enamel)}$ value on M1 than on M2 (Fig. 4), which is an opposite pattern to what one can expect in case of a consumption of breast milk and then a weaning during the first years of life. Moreover, US215/Mand1 M1 exhibits a far higher value than the other SSPM population M2s (mean = -3.7 ± 1.1‰) (Fig. 6). The $\delta^{18}O_{sc\ (enamel)}$ difference between US215/Mand1 M1 and the SSPM population M2s is 5‰, and greatly exceeds the mean ^{18}O-enrichment of M1s caused by nursing.

Food and beverage processing could have influenced the $\delta^{18}O_{sc}$ signals recorded in US215/Mand1 enamel samples. Culture-specific culinary and dietary practices can be responsible of sizeable modifications of the original stable isotope compositions of water in food and beverages (Brettell et

al., 2012; Britton et al., 2015; Daux et al., 2008; Warinner and Tuross, 2009). Recent experiments highlighted that specific cooking processes may shift the $\delta^{18}O$ values of food resources up to +5.2‰ (e.g. Royer et al., 2017). In a lower degree, beverage production techniques and storage may increase the $\delta^{18}O$ values of the initially used water up to +1.3‰ (e.g. Brettell et al., 2012; Spangenberg and Vennemann, 2008). If food water and drinking liquids contribute together to the final oxygen isotopic composition of consumer's body tissues, the former contributes much less than the latter to this signal. Thus, the shifted $\delta^{18}O$ values of food would be mitigated by those of beverages. Both would be in turn balanced by the $\delta^{18}O$ values of raw food and unprocessed drinking liquids (Brettell et al., 2012; Royer et al., 2017). The final influence on the $\delta^{18}O_{sc}$ values, even in the hypothesis of a cumulative effect, would be therefore well below the discrepancy observed between US215/Mand1 M1 and the mean value of SSPM population M2s. Besides, culinary practices of Romans were assuredly diverse (André, 2009; Hilgers, 1969), and a mix of isotopic shifts in processed food and beverages would be expected, which would necessarily reduce the effect of the most extreme offsets induced by certain cooking methods. Furthermore, dietary habits are culturally mediated behaviors. Thus, the latter should be shared by not only one individual but the entire group, which is clearly not the case in the SSPM catacombs.

A different origin from the rest of the SSPM population appears therefore the most plausible explanation for the atypical $\delta^{18}O_{sc\ (enamel)}$ values of US215/Mand1. Such high $\delta^{18}O$ values would indicate that this individual is originated from a region characterized by a much warmer, drier climate than Lazio. US215/Mand1 seems, however, to have moved in this region during their early life. While M1 and M3 have similar $\delta^{18}O_{sc\ (enamel)}$ values, they both differ from M2 by about 1‰. This difference suggests that US215/Mand1 either experienced a circular migration (between two different locations) or had a complex migration trajectory (with several changes of residences) during their childhood/adolescence in the above-described region. With a $\delta^{18}O_{sc\ (bone)}$ value falling within one standard deviation from the population mean value, US215/Mand1 would have, however, inhabited several years in Rome to record the local $\delta^{18}O$ signature in bone (Fig. 4). Furthermore, this result allows us to assign an age to this individual, which was unknown so far. Based on the differences of $\delta^{18}O_{sc}$ values between teeth and bone, and taking into account the rhythms of bone turnover, it can be established that US215/Mand1 was an adult. It can also be concluded that US215/Mand1 spent their life in a geological zone similar to the area of Rome, or at least a region with analogous $^{87}Sr/^{86}Sr$ ratios to the region of Rome, during the formation of the three molars.

US215/Mand1 presents $\delta^{13}C_{sc\ (enamel)}$ values of -12.9‰, -12.5‰ and -12.3‰ for M1, M2 and M3, respectively (Table 3). Their mandible bone sample exhibits $\delta^{13}C_{col}$, $\delta^{15}N_{col}$, $\delta^{34}S_{col}$, and $\delta^{13}C_{sc\ (bone)}$ values of -19.0‰, +12.5‰, +8.4‰, and -13.9‰, respectively (Table 3; Fig. 7 and 8). Taking into account the average carbon offsets between a consumer's tissues and diet (Bocherens and Drucker, 2003;

Fernandes et al., 2012; Howland et al., 2003; Passey et al., 2005; Salesse, 2015; Warinner and Tuross, 2009), a $\delta^{13}C_{diet}$ value of about -26/-24‰ can be estimated.

The estimated $\delta^{13}C_{diet}$ value is close to the mean $\delta^{13}C_{C3\ plants}$ value, suggesting that US215 had a diet predominantly based on C_3 terrestrial plant and herbivorous animal resources. In addition, the $\delta^{15}N_{col}$ value (Fig. 7) is higher than the upper end of the common range for C_3 terrestrial consumers (Bocherens and Drucker, 2003; Chisholm et al., 1982; Hedges and Reynard, 2007; Schoeninger et al., 1983), indicating the inclusion of organisms with relatively high trophic levels, such as aquatic resources (Craig et al., 2010; Drucker et al., 2005; Richards et al., 2015). With a $\delta^{34}S_{col}$ value falling into the range for terrestrial/freshwater consumers (Fig. 7) (Nehlich, 2015; Peterson et al., 1985; Tsutaya et al., 2019), a consumption of marine food sources can be discarded. Freshwater fish was most likely the aquatic resource served at US215/Mand1's table. Thus, a mixed diet relying on the triad C_3 plants / C_3 herbivore meat / freshwater fish products was consumed by this individual.

The US215/Mand1's dietary pattern is shared by a small batch of individuals from the Region X of the SSPM catacombs (Salesse, 2015) but also by individuals from at least two other contemporaneous populations from Rome [Catacombs of St. Callixtus (Rutgers et al., 2009); Tenuta des Duca (O'Connell et al., 2019)] (Fig. 8). Moreover, if aquatic resources are considered regardless the environment from which they originate, fish consumers are commonly identified in the Roman populations from Lazio. Diets based on aquatic resources (only marine, both freshwater and marine, or without differentiation) have been proposed as an explanation for individuals presenting high $\delta^{15}N_{col}$ values at Castellaccio Europarco and Casal Bertone (Killgrove and Tykot, 2013), Gabii (Killgrove and Tykot, 2018), Casale del Dolce and Osteria della Fontana (Nitsch, 2012), and SSPM catacombs (Nitsch, 2012; Salesse, 2015), Isola Sacra and ANAS (Prowse et al., 2004), and finally Lucus Feroniae (Tafuri et al., 2018) (Fig. 8). With a $\delta^{15}N_{col}$ value of 12.5‰, US215/Mand1 stands among the top 10% of individuals with the most elevated $\delta^{15}N_{col}$ values in Lazio ($n_{10\%} = 60$; $n_{total} = 603$) (Fig. 8). Apart a possible consumption of aquatic resources, the individuals from this top 10% group are characterized by high protein intakes. Aquatic resources, referring to fish in particular, contain generally more proteins than terrestrial animal source food (FAO, 1989; Heinz and Heutzinger, 2007; Moharrery, 2007). A consumer of aquatic products, such as US215/Mand1, has therefore a protein-rich diet.

Based on these findings, a dietary scenario including C_3 plants, C_3 terrestrial domesticated herbivores and freshwater fish was tested through Bayesian modelling. The Bayesian approach suggests that US215/Mand1 would have consumed 63 ± 13% of terrestrial plant cereals, 18 ± 12% of meat of terrestrial animals, and 19 ± 9% of meat of freshwater fish. It estimates also that their diet would have been composed of about 28% of proteins and 72% of carbohydrates/fats. However, due to a limited baseline, this diet reconstruction must be considered as a tentative explanation, providing orders of magnitude. Nevertheless, the Bayesian mixing model highlights once again that

US215/Mand1 consumed terrestrial meat and aquatic resources in similar proportions and had a high protein intake.

5.2. Inferring the ancestry and origin of US215/Mand1 through dental morphology

The full list of recorded traits was analyzed for inter-trait correlation using Kendall tau-b, which led to the exclusion of the C1-C2 crest and the mandibular pit tubercle on the second lower molar ($r = 1.00$, $n = 8$, no p-value was generated). The entoconulid, metaconulid and distal fossa prevalence rates exhibited no variation within the sample (0% present). An intra-observer error test by the data collector ($r = 0.978$, $p < 0.001$, $n = 216$) has shown good agreement between observation events (Maaranen et al., 2019).

The analysis was performed on the SSPM individuals (Table 1) using 11 traits, retained after the inter-trait correlation test (Table 2). Though some of traits can be recorded in a scale, they were treated as binary if present only in grade 1 (e.g. the protostylid, presented only as a buccal pit described by Scott and Irish, 2017). Lower third molar absence, torsomolar angle and crenulation were only present in one individual per trait, so they were treated as asymmetric binary variables. How traits were treated is included in Table 1 and the full data and distance matrix in Tables C1 and C2.

A two-dimensional NMDS plot was created (Fig. 9). US215/Mand1 and US216/Mand2 resided far from the centroid, the former falling beyond the 90% confidence level and the latter even beyond 95%. Factor analysis indicated that most of the variation was contributed to enamel extension, anterior fovea, hypocone size, crenulation and deflecting wrinkle (altogether circa 60%). A hierarchical cluster analysis using complete-linkages also suggests the two individuals cluster away from the others (Fig. 10).

To explore the data further from a morphological perspective, the data was divided into clusters using the function pam from the R package cluster. Silhouette method indicated an optimal number of 5 clusters (Fig. C1). The clusters were used as group indicators in the second visualization technique, t-SNE (Fig. C2), indicating that US215/Mand1 and US216/Mand2 formed their own morphological groups. The data suggest that there is heterogeneity in the SSPM dataset, with US215/Mand1 and US216/Mand2 even more morphologically different from the other individuals. Hierarchical clustering places the two individuals close to one another, but the cluster analysis divides them even from each other. It is pertinent to remember that the results are tentative, given the analysis was conducted using three molars and altogether 11 variables (Table 2). Crenulation was observed on the lower molars of US215/Mand1 but none of the other individuals in the SSPM sample.

Only five individuals from the SSPM catacombs were appropriate for the geometric morphometric outline analysis (Fig. 11). Analysis on the molar outline did not produce clustering (Fig. 11) which is

probably due to small sample size. PC1 and PC2 explain 52% and 28% of the variation (cumulative 80%). Again, individuals US215/Mand1 and US216/Mand2 are separate but not significantly (ANOVA effect size; Z = 0.17, p = 0.46), unsurprising given the distance between the individuals along PC1. Most of the variation in the shape was captured in the lower third molar (Fig. C3), the most variable tooth in the dentition. The inherent variation of this tooth could explain why each configuration was so different, which coupled with the small sample size could not generate meaningful clusters.

5.3. aDNA, an attempt to address the provenance of US215/Mand1

No Y-chromosome SNPs could be characterized for any of the targeted samples, and very rare mitochondrial SNPs were obtained (Supplementary File D). Mitochondrial results were conclusive only for the sample US219/Mand1 from the chamber X83 to which replicable haplogroup H1 could be assigned (Supplementary File C). The latter cannot be, however, specified with the type of investigation applied here. Haplogroup H is the most common in today's Europe, and for example reach 38.99% in Italy (Turchi et al., 2008). As the current repartition of the sub-haplogroup H1 covers Europe as well as North Africa (Gleize et al., 2016), it cannot give a more precise information for the origin of individual US219/Mand1, who could come from Italy as well as from other European or North African regions. The other mitochondrial results were either non-replicable (Sq108 from X83), or inconsistent (US215/Mand1 from X83), or too scarce (n°13/Mand1 from X81; Sq152 and US219/Mand2 from X83) (Supplementary File C). The aDNA analyses clearly demonstrated a major DNA degradation in the specific case of these individuals, which could easily be explained by the environmental conditions inside the SSPM catacombs combined to specific funerary treatments (presence of lime) highly detrimental to DNA preservation.

6. DISCUSSION

If regional-scale predictive $^{87}Sr/^{86}Sr$ maps for southern Europe, Near East and North Africa are still missing, global and regional $\delta^{18}O$ isoscapes are available for the areas covered by the Roman Empire at its greatest extent (i.e. during the 2nd century AD). Based on the OIPC maps (http://wateriso.utah.edu/waterisotopes/pages/data_access/figures.html), three locations inside or in the immediate vicinity of the Roman Empire can be identified as potential regions of origin for US215/Mand1: the Arabian Peninsula, the Nile Valley and within the central Sahara Desert.

Measurements on modern rivers waters but also on archaeological human and faunal remains sampled in these three regions corroborate the predictive $\delta^{18}O$ models. Upstream at Khartoum, Farah

et al. (2000) and Iacumin et al. (2016) determined mean $\delta^{18}O_{water}$ values for the main Nile of +2.5‰ and +1.8‰, respectively. Similarly, downstream at Cairo, Buzon and Bowen (2010) reported a mean $\delta^{18}O_{water}$ value for the Nile River of +2.3‰. In a synthesis effort, Dufour et al. (2018) showed that the $\delta^{18}O_{water}$ values could, however, vary a bit all along the river. Nevertheless, the $\delta^{18}O_{water}$ values for the Nile would have remained broadly stable from the Late Period of ancient Egypt/the Meroitic Period in Sudan to nowadays (Touzeau et al., 2013). This is mainly supported by the high and positive $\delta^{18}O$ values displayed by human and animal samples during that time span (Buzon et al., 2019; Iacumin et al., 1996; Iacumin et al., 2016; Touzeau et al., 2013). Also, oxygen isotope compositions of tooth enamel from archaeological faunal specimens collected in the Libyan Sahara are in good accordance with the $\delta^{18}O$ values of modern precipitations (di Lernia et al., 2013). Besides, the variations of $\delta^{18}O_{sc\ (enamel)}$ values suggest that US215/Mand1 spent their early life to change of residences in one of these three regions.

From a dental morphological perspective, US215/Mand1 differs from the rest of the SSPM population (Fig. 9, 10, 11 and C2). Furthermore, the unique presence and high expression (grades ≥ 1 for M1 and M2; grade = 2 for M3) of crenulations on the US215/Mand1's molars are of particular interest as they could be informative of a specific population history. This dental nonmetric trait has notably been identified as being more common among African and African-derived populations (Pilloud et al., 2018; Rhine, 1990). Especially, Pilloud and colleagues (2018) established that there was a relationship between the presence of grades equal to or greater than 1 and the modern American Black and South African samples they studied. Therefore, the complex molar surfaces as well as the molar crenulation trait presence would support an African ancestry of US215/Mand1.

After excluding outliers (Grubb's tests), the $^{87}Sr/^{86}Sr$ ratios display by humans vary from 0.70731 to 0.70807 in Egypt, from 0.70658 to 0.70912 in Sudan, and from 0.70975 to 0.71293 in central Sahara Desert (Fig. 12) (Tafuri et al. 2006; Buzon et al., 2007; Sereno et al., 2008; Buzon and Simonetti, 2013; di Lernia and Tafuri, 2013; di Lernia et al., 2013; Stojanowski and Knudson, 2014; Schrader et al., 2019). Based on these data, neither the northern part of the Nile Valley nor the Saharan area appear to be places from where US215/Mand1 could originate. Moreover, if at first glance the Third Cataract region could be a possible origin for US215/Mand1 (core $^{87}Sr/^{86}Sr$ range = 0.70696-0.70912; Fig. 12), Buzon and colleagues have suggested that individuals with $^{87}Sr/^{86}Sr$ values greater than 0.70783 did not belong to this locality but were migrants from northern lands (Buzon and Simonetti, 2013; Buzon et al., 2016). Among the latter stands the Second Cataract region. Because of its geological complexity, this region presents a large local $^{87}Sr/^{86}Sr$ range, varying between 0.704 and 0.717 (Schrader et al., 2019). Animal samples recovered near the Second Cataract exhibit a wide distribution of their $^{87}Sr/^{86}Sr$ values as well, ranging between 0.70667 and 0.70933 (after removing outliers via Grubb's test) (Fig. 12). This represents a pertinent area where US215/Mand1 could have spent their early life. Additionally, cattle from Nubian sites show generally a broad range of $^{87}Sr/^{86}Sr$ values (Fig. 12), which

suggests that imports and/or transhumance of some animals may have occurred (Buzon and Simonetti, 2013; Schrader et al., 2019). Non-local cattle were most probably brought from surrounding regions as tributes or traded with communities – either nomadic or not – from the arid desert edge (Buzon and Simonetti, 2013; Iacumin et al., 2001; Thompson et al., 2008). Thus, cattle Sr variability would indicate that various – unknown – localities from Sudan could have been possible places of origin for US215/Mand1. Even though available $^{87}Sr/^{86}Sr$ values for humans from central Sahara Desert do not fit with those of US215/Mand1, one could be intrigued by the isotopic composition of an equid specimen recovered in the Messak Mountains (di Lernia et al., 2013). Of the two measurements taken along its M3 crown, one is similar to the $^{87}Sr/^{86}Sr$ values exhibited by US215/Mand1 ($^{87}Sr/^{86}Sr_{MK07/39C1\text{-}09}$ = 0.7087 in di Lernia et al. (2013)) (Fig. 12). If this animal moved in that region, it also suggests that the central Sahara Desert cannot be excluded as a potential origin of US215/Mand1.

Together these lines of evidence converge and argue for an origin beyond the African Roman frontier for US215/Mand1, making this individual the first example of an African-born migrant revealed by a multi-analytical approach including isotopic analysis and discovered in the Imperial capital. Moreover, US215/Mand1 has experienced the second longest migration across the Roman Empire highlighted by direct evidence, after the one discovered in Roman York (UK) discussed by Martiniano et al. (2016) who suggested a Middle Eastern origin based on genomic and isotope data.

Fish, whether marine or freshwater, was a social marker at the time of the imperial era (André, 2009). While there are many indications that rich and poor alike had access to resources of the same nature, they did have different dietary practices (André, 2009; Garnsey and Saller, 1987; Schirmer, 2014; Spurr, 1983). The quality but also the diversity of the food consumed, as well as the way it was prepared, varied considerably between the low and high strata of Roman society (André, 2009; Purcell, 1995; Schirmer, 2014). Freshwater fish, in Rome as in other parts of the Empire, was consumed in large quantities only by the most humble or ordinary people (André, 2009; Marzano, 2018). The wealthier individuals and elites would occasionally consume it, but undoubtedly preferred marine fish. In addition to their taste, marine fish also represented a potent sign of wealth. In short, fish, whether marine or freshwater, was a social marker at the time of the imperial era (see André, 2009 and Marzano, 2018 for thorough historical syntheses). Based on the isotopic results showing US215/Mand1 consuming freshwater fish in a significant proportion, one can suggest that US215/Mand1 had probably a modest socio-economic status and belonged to the low strata of the Roman society.

These different lines of evidence support two storylines for US215/Mand1. The least likely would be that US215/Mand1 was a free man or woman originated from the northern part of the African continent, who would have settled in the city of Rome for specific business. The most likely would be that after spending their early life moving in the vicinity of the Nile Valley or within the central Sahara Desert, possibly due to a nomadic condition or a peregrine status, US215/Mand1 could have

experienced forced migration as a slave and was eventually shipped to Rome along trade routes. On the basis of the evidence we have, it is unfortunately impossible to assess whether US215/Mand1 belonged to a private household or was owned by Rome's people, acting as a public slave. More broadly, the presence of US215/Mand1 in the mass graves of the SSPM catacombs provides a better understanding of the epidemic. As it seems that individuals from all strata of Rome were buried together in these sepulchral spaces, the epidemic was not selective from a socio-economic point of view. This would confirm the snapshot and the uncommon nature of this archaeological context.

7. CONCLUSION

Based on a multi-tissue sampling strategy including molar teeth and mandibular cortical bone, our multi-analytical approach using isotopic ($\delta^{13}C$, $\delta^{15}N$, $\delta^{18}O$, $\delta^{34}S$, $^{87}Sr/^{86}Sr$), dental morphology (geometric morphometrics, nonmetric traits) and ancient DNA (mitochondrial DNA, Y chromosome) analyses has refined the origin and life history of US215/Mand1 buried in the X83 mass grave from the SSPM catacombs. Obtained lines of evidence suggest that this individual was born beyond the southern *limes*, possibly in the vicinity of the Nile Valley or within the central Sahara Desert, and experienced diachronic changes of residence during their early life, conceivably due to a nomadic condition or a peregrine status. The way US215/Mand1 arrived in the imperial capital is still hypothetical, although it seems likely that he/she could have undergone forced migration and eventually transported as a slave to Rome. It cannot be totally excluded, however, that US215/Mand1 was a free man or woman originated from North Africa, settling in the city of Rome for specific business affairs. This study presents direct evidence of one of the unique cases of long-distance migration across the Empire of a non-Roman. In particular, it highlights for the first time the journey of a North African-born individual who died in the Eternal city. Enslaved or not, US215/Mand1 clearly illustrates and confirms the cosmopolitan character of Rome. Finally, this study restates the importance and usefulness of multi-proxy investigations for reconstructing the identities of past human individuals recovered in archaeological contexts.

ACKNOWLEDGMENTS

The main author wishes to express his gratitude to R. Giuliani, chief inspector of the Vatican's Pontificia Commissione di Archeologia Sacra for the material authorization. The main author thanks J. Ughetto-Monfrin (SSMIM, France), C. Wurster (James Cook University, Australia) and J. Wilson (University of South Florida, USA) for their support with the stable isotope analysis. The main author

656 acknowledges C. Snoeck (Vrije Universiteit Brussel, Belgium) for useful discussions. Finally, all the
657 authors are grateful to the editors and reviewers for their time and constructive comments on our
658 manuscript.
659
660 **FUNDING**
661
662 Funding was generously supplied by the Aquitaine Region (France) and the Maison des Sciences
663 de l'Homme d'Aquitaine (Pessac, France) through the project "L'église, les vivants, les morts", the
664 Action Thématique du MNHN "Biomineralization" (Paris, France), the International Catacomb Society
665 through its Shohet Scholars Grant Program "Quantifying the Roman diet" (Boston, USA).

FIGURES

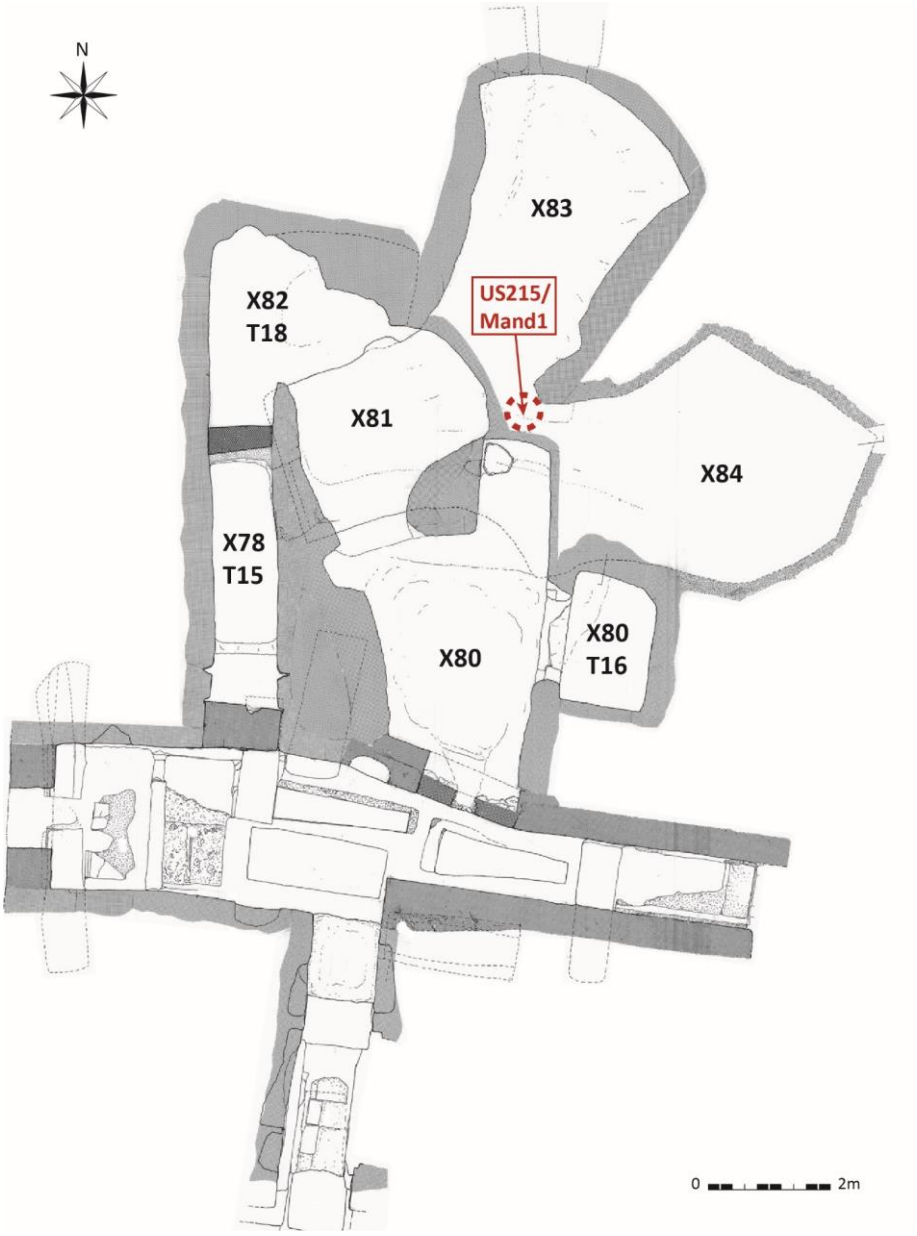

Fig. 1. Map of the burial chambers in the SSPM catacombs. Note: The dotted circle indicates the location where the support pillar has been built and US215/Mand1 have been recovered. Modified after M. Ricciardi in Castex and Blanchard 2011.

Fig. 2. Picture showing the support pillar newly built as well as the burials chambers X83 (left) and X84 (right) in the background. Note: Picture of D. Gliksman/INRAP.

Fig. 3. Preserved right hemi-mandible fragment of US215/Mand1.

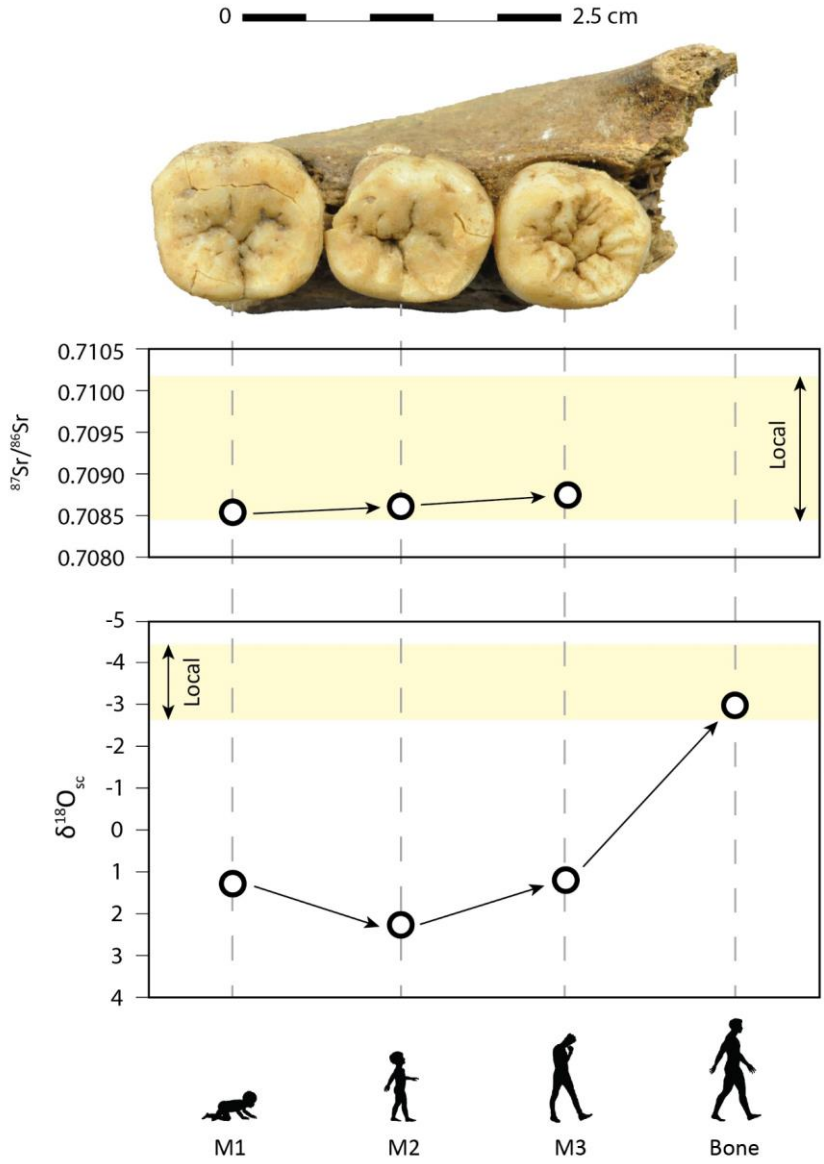

Fig. 4. Variation of the $^{87}Sr/^{86}Sr_{enamel}$, $\delta^{18}O_{sc\ (enamel)}$ and $\delta^{18}O_{sc\ (bone)}$ values in US215/Mand1. Note: 'M1', 'M2' and 'M3' stands for permanent molars 1, 2 and 3, respectively. The yellow area corresponds to the local range defined as one standard deviation from the SSPM population mean. The standard deviation between replicates is inferior to size of dots.

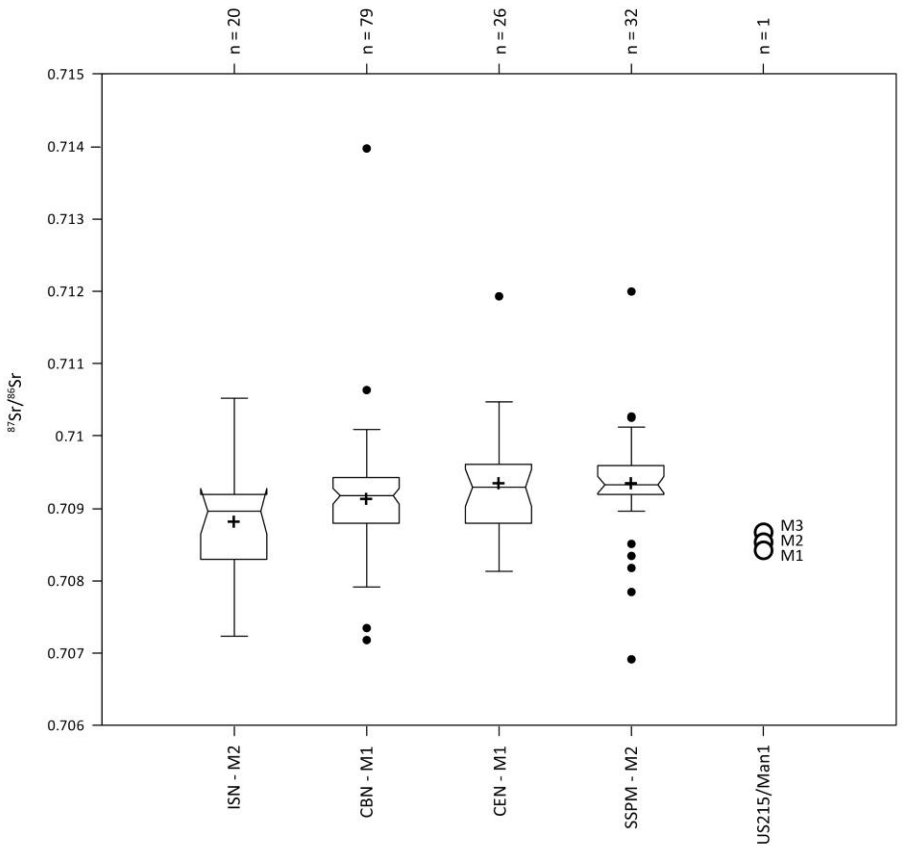

683

684 **Fig. 5.** Inter-site comparison of the $^{87}Sr/^{86}Sr$ ratios measured on human dental samples from the Rome's region.
685 Note: 'M1' and 'M2' stands for permanent molars 1 and 2, respectively. 'ISN' refers to Isola Sacra Necropolis,
686 'CBN' to Casal Bertone Necropolis, 'CEN' to Castellaccio Europarco Necropolis, and 'SSPM' to Saints Peter and
687 Marcellinus catacombs. Bibliographic references: Salesse (2015), Killgrove and Montgomery (2016), Stark (2017).
688 The boxes depict groups of data through their quartiles.

689

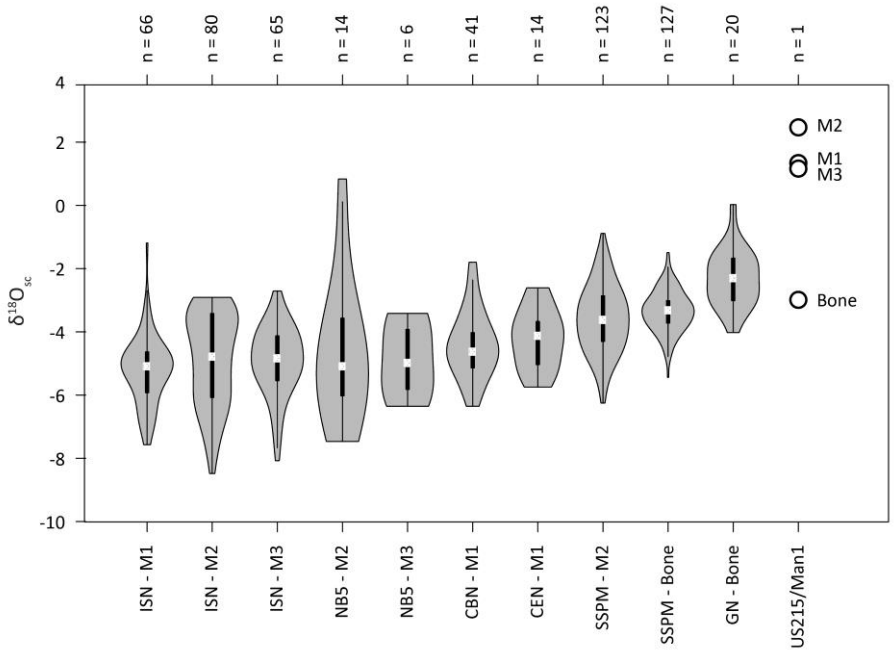

690

691 **Fig. 6.** Inter-site comparison of the $\delta^{18}O_{sc}$ values measured on human dental samples from the Rome's region.
692 Note: 'M1', 'M2' and 'M3' stands for permanent molars 1, 2 and 3, respectively. 'ISN' refers to Isola Sacra
693 Necropolis, 'NB5' to Navalia Building 5, 'CBN' to Casal Bertone Necropolis, 'CEN' to Castellaccio Europarco
694 Necropolis, 'GN' to Gabii Necropolis, and 'SSPM' to Saints Peter and Marcellinus catacombs. Bibliographic
695 references: Prowse 2001, Prowse et al. 2007, Salesse (2015), Killgrove and Montgomery (2016), Stark (2017),
696 Killgrove and Tykot (2018), O'Connell et al. (2019). The violins show the probability density of the data at different
697 values, smoothed by a kernel density estimator. The boxes depict groups of data through their quartiles.
698

699

700

701

702

703

704

705

706

707

708

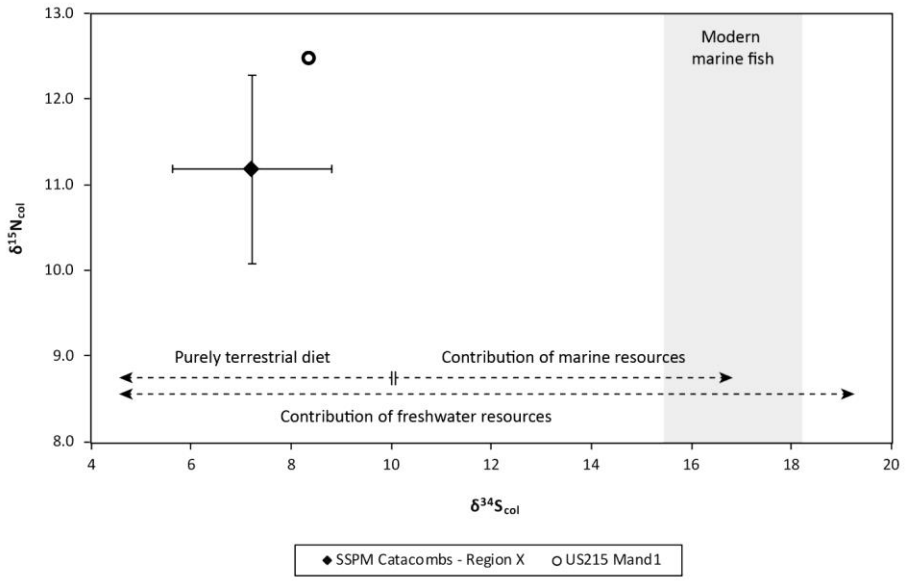

709

710 **Fig. 7.** Biplot of the $\delta^{34}S_{col}$ and $\delta^{15}N_{col}$ values measured on bone samples from the SSPM individuals. Note: The
711 shaded area corresponds to the range of $\delta^{34}S_{col}$ values for modern marine fish. The arrows indicate where
712 individuals should stand according to their diet.

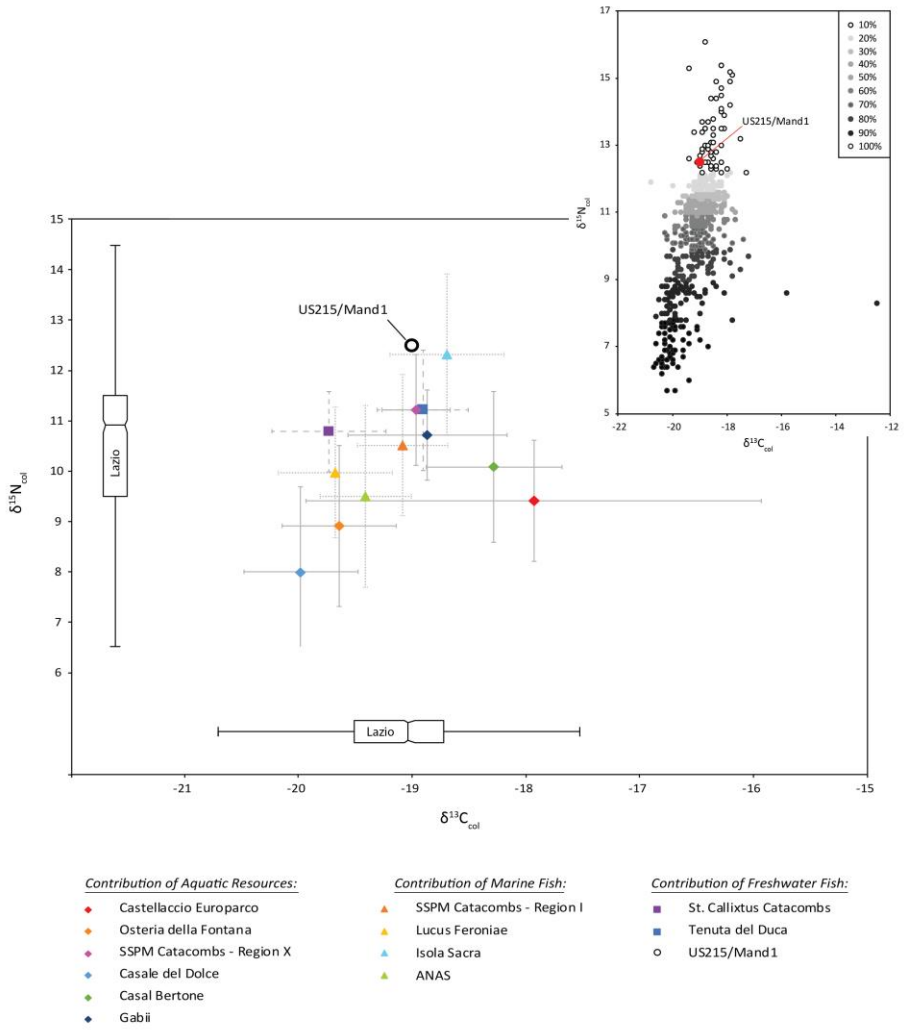

Fig. 8. Biplots of the $\delta^{13}C_{col}$ and $\delta^{15}N_{col}$ values (mean ± 1 SD) measured on human bone samples from Lazio. Note: The classification of the populations is based on the interpretations proposed by Prowse et al. (2004), Rutgers et al. (2009), Nitsch (2012), Killgrove and Tykot (2013, 2018), Salesse (2015), Tafuri et al. (2018), O'Connell et al. (2019). The boxes show the regional variability of the isotopic values. Color gradient of the scatter plot in the top right corner is based on the $\delta^{15}N_{col}$ values.

Formatted: Danish

Formatted: English (United Kingdom)

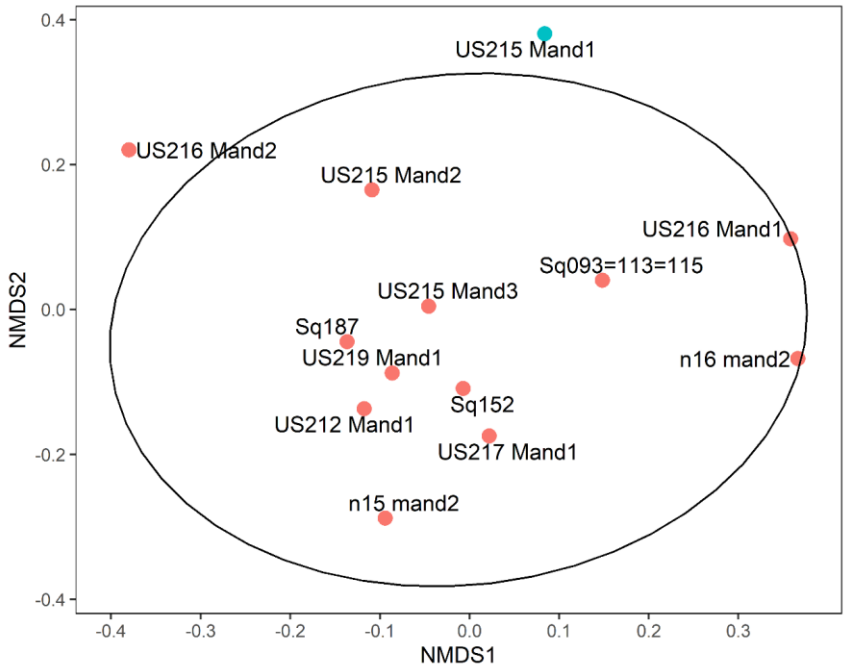

722

723 **Fig. 9.** NMDS plot was created from the distance matrix (see Table C2) of the SSPM individuals. The ellipse marks
724 the 90% confidence level for the sample. Both US215 Mand1 and US216 Mand2 fall far away from the rest of the
725 individuals.
726

727

728

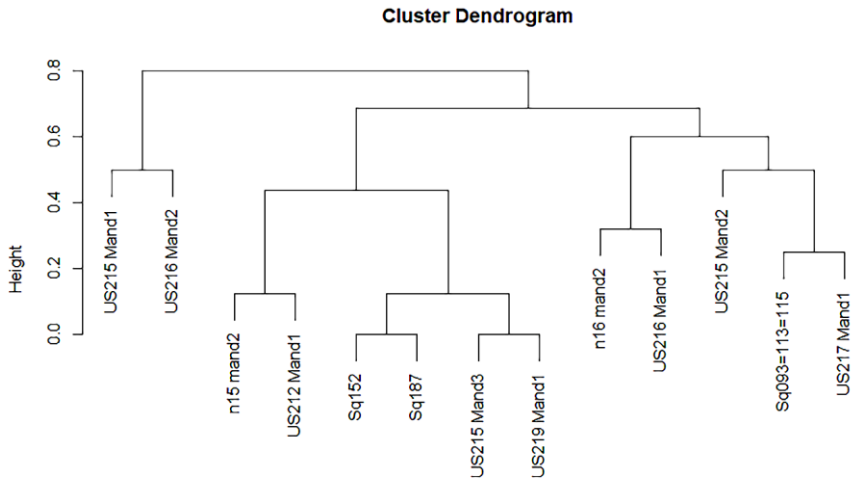

729

730 **Fig. 10.** Hierarchical dendrogram generated from the SSPM non-metric dental dataset. Note: The agglomerative
731 method complete linkage was used. US215/Mand1 (ID 206) and US216/Mand2 (ID 210) are separated from the
732 rest.

733

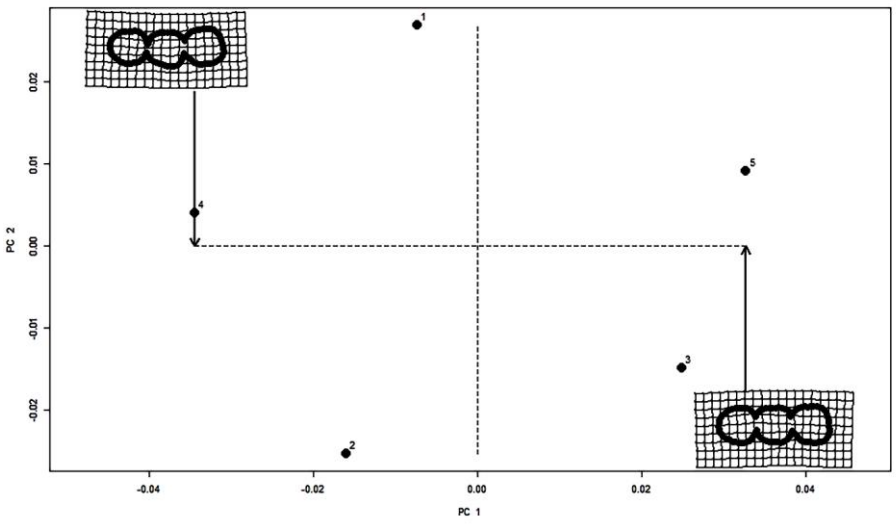

734

735 **Fig. 11.** PCA plot performed on the geometric morphometric data obtained on the SSPM individuals. Note: PC1
736 explains 52% of the shape variation, and PC2 28%. ID1=X81_n°14/Mand2, ID2=X83_US215/Mand1,
737 ID3=X83_US216/Mand2, ID4=X83_US217/Mand1, and ID5=X83_US219/Mand1.

738

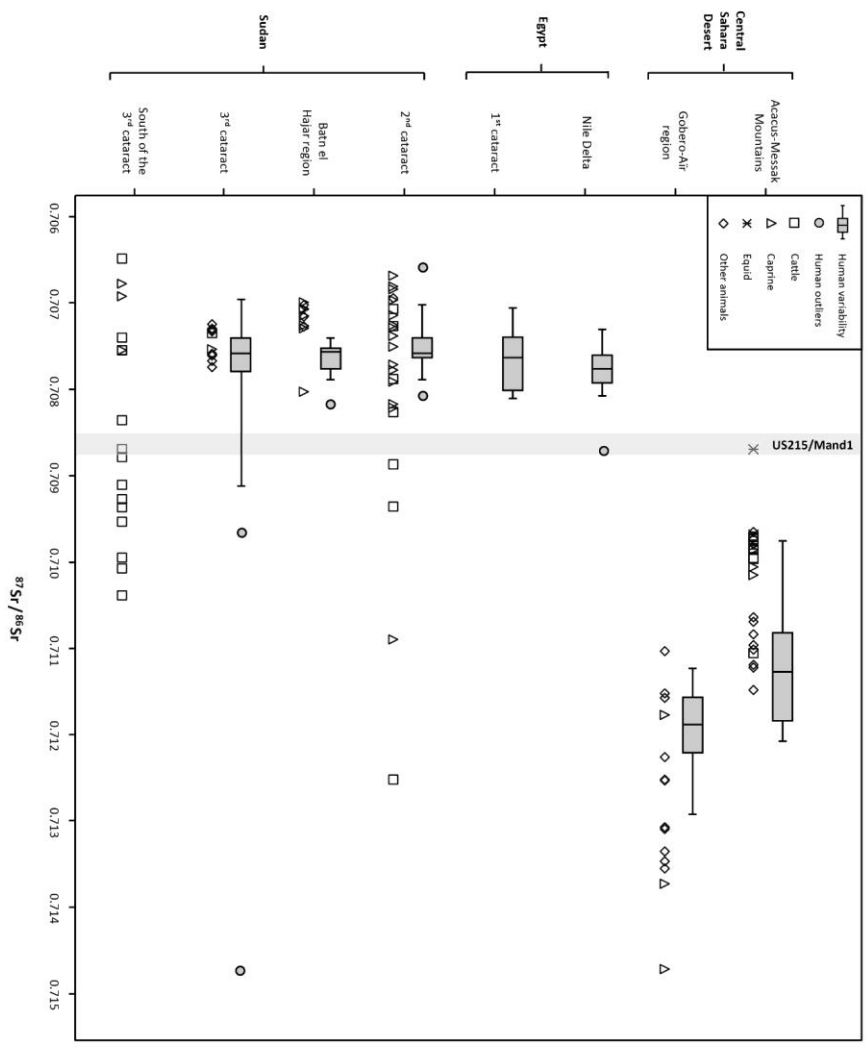

739

740 **Fig. 12.** Variability of the $^{87}Sr/^{86}Sr$ ratios measured on human and faunal remains from North African region.
741 Bibliographic references: Tafuri et al. (2006), Sereno et al. (2008), di Lernia and Tafuri (2013), di Lernia et al.
742 (2013), Stojanowski and Knudson (2014) for Central Sahara Desert; Buzon et al. (2007), Buzon and Simonetti
743 (2013), Schrader et al. (2019) for Egypt-Sudan. Note: Populations dates from different times periods. Boxes
744 represent the range of variation of human values. Outliers have been identified through Grubb's tests. The
745 shaded area corresponds to the range of $^{87}Sr/^{86}Sr$ values exhibit by the molars of US215/Mand1.

Formatted: Danish

TABLES

Table 1. Individuals used in the biodistance (based on dental traits (DT)), geometric morphometrics (GM) and DNA analyses.

DT ID	GM ID	DNA ID	Room/Site	Individual	Sex	Age
-	-	**1**	X81	n°13/Mand1	U	11.8+
-	**1**	-	X81	n°14/Mand2	U	16.4+
101	-	-	X81	n°15/Mand2	U	-
102	-	-	X81	n°16/Mand2	U	11.8+
-	-	**2**	X83	Sq108	F	15-19
203	-	-	X83	Sq093=113=115	U	20+
204	-	**3**	X83	Sq152	U	20+
205	-	-	X83	US212/Mand1	U	8.7+
206	**2**	**4**	X83	US215/Mand1	U	16.4+
207	-	-	X83	US215/Mand2	U	16.4+
208	-	-	X83	US215/Mand3	U	16.4+
209	-	-	X83	US216/Mand1	U	14.8+
210	**3**	-	X83	US216/Mand2	U	16.4+
211	**4**	-	X83	US217/Mand1	U	16.4+
212	**5**	**5**	X83	US219/Mand1	U	16.4+
-	-	**6**	X83	US219/Mand2	U	11.8+
313	-	-	X84	Sq187	F?	15-19

Table 2. Traits used to investigate biodistance.

Trait	Abbr.	Tooth	Reference	Type	n
Protostylid	PR	LM1	Scott and Irish, 2017	Binary	5
Deflecting wrinkle	DW	LM1	Scott and Irish, 2017	Ordinal	9
Hypoconulid	C5	LM2	Scott and Irish, 2017	Ordinal	10
Groove pattern (present=y)	GP	LM2	Scott and Irish, 2017	Binary	13
Anterior fossa	AF	LM2	Scott and Irish, 2017	Ordinal	12
Enamel extension	EE	LM2	Scott and Irish, 2017	Ordinal	13
Root number	R	LM2	Scott and Irish, 2017	Ordinal	8
Crenulation	C	LM2	Pilloud et al., 2018	Binary	8
Lower third molar absence	UM3V	LM3	Scott and Irish, 2017	Binary	12
Mandibular molar pit tubercle	MPT	LM3	Marado and Silva, 2016	Ordinal	8
Torsomolar angle	TA	LM3	Scott and Irish, 2017	Binary	9

Note: 'Abbr.' stands for abbreviation. 'Tooth' refers to teeth selected to represent the trait. 'Type' refers to the way the trait was coded into the software. 'n' indicates the overall number of observations from the SSPM individuals.

Table 3. Stable isotope results for reconstruction dietary patterns of US215/Mand1.

US215/Mand1 - Diet													
Molar teeth			Mandibular bone										
M1	M2	M3											
$\delta^{13}C_{carb}$	$\delta^{13}C_{carb}$	$\delta^{13}C_{carb}$	%Col	%C	%N	%S	C:N	C:S	N:S	$\delta^{13}C_{col}$	$\delta^{15}N_{col}$	$\delta^{34}S_{col}$	$\delta^{13}C_{carb}$
-12.9	-12.5	-12.3	6.7	38.5	13.6	0.31	3.3	331.2	100.3	-19.0	+12.5	+8.4	-13.9

Table 4. Stable isotope results for discussing the mobility of US215/Mand1.

US215/Mand1 - Mobility										
Molar teeth									Mandibular bone	
M1			M2			M3				
$\delta^{18}O_{carb}$	$\delta^{18}O_{dw}$	$^{87}Sr/^{86}Sr$	$\delta^{18}O_{carb}$	$\delta^{18}O_{dw}$	$^{87}Sr/^{86}Sr$	$\delta^{18}O_{carb}$	$\delta^{18}O_{dw}$	$^{87}Sr/^{86}Sr$	$\delta^{18}O_{carb}$	$\delta^{18}O_{dw}$
+1.3	+0.9	0.7085	+2.3	+2.6	0.7086	+1.2	+0.7	0.7087	-3.0	-4.4

Note: See section 4.1.4 for the conversion procedures to estimate the $\delta^{18}O_{dw}$ values.

REFERENCES

Abrecht, R.R., 2019. An immigrant neighbourhood in ancient Rome. Urban History, 1-21.

Alvarez, H.P., 2000. Grandmother hypothesis and primate life histories. American Journal of Physical Anthropology 113, 435-450.

Ambrose, S.H., 1990. Preparation and characterization of bone and tooth collagen for isotopic analysis. Journal of Archaeological Science 17, 431-451.

André, J., 2009. L'alimentation et la cuisine à Rome. Les Belles Lettres, Paris.

Balasse, M., Ambrose, S.H., Smith, A.B., Price, T.D., 2002. The seasonal mobility model for prehistoric herders in the south-western Cape of South Africa assessed by isotopic analysis of sheep tooth enamel. Journal of Archaeological Science 29, 917-932.

Balter, V., Lécuyer, C., 2010. Determination of Sr and Ba partition coefficients between apatite from fish (Sparus aurata) and seawater: the influence of temperature. Geochimica et Cosmochimica 74, 3449-3458.

Blanchard, P., Castex, D., Coquerelle, M., Giuliani, R., Ricciardi, M., 2007. A mass grave from the catacomb of Saints Peter and Marcellinus in Rome, second-third century AD Antiquity 81, 989-998.

Blanchard, P., Réveillas, H., Kacki, S., Castex, D., 2015. La catacombe des Saints Pierre-et-Marcellin à Rome (I^{er}-III^{e} s.) : discussion sur l'origine des défunts et leur décès, in: Branco, G., Rocha, L., Duarte, C., de Oliveira, J., Ramírez, B. (Eds.), Arqueologia de Transição: O Mundo Funerário. Actas do II Congresso Internacional Sobre Arqueologia de Transição (29 de Abril a 1 de Maio 2013). CHAIA, Évora, pp. 197-216.

Bocherens, H., Drucker, D.G., Taubald, H., 2011. Preservation of bone collagen sulphur isotopic compositions in an early Holocene river-bank archaeological site. Palaeogeography, Palaeoclimatology, Palaeoecology 310, 32-38.

Bocherens, H., Fizet, M., Cuif, J.P., Jaeger, J.-J., Michard, J.-G., Mariotti, A., 1988. Premières mesures d'abondances isotopiques naturelles en ^{13}C et en ^{15}N de la matière organique fossile de dinosaure. Application à l'étude du régime alimentaire du genre *Anatosaurus* (*Ornithischia, Hadrosauridae*). Comptes Rendus de l'Académie des Sciences 306, 1521-1526.

Bocherens, H., Fizet, M., Mariotti, A., Lange-Badre, B., Vandermeersch, B., Borel, J.P., Bellon, G., 1991. Isotopic biogeochemistry (^{13}C, ^{15}N) of fossil vertebrate collagen: application to the study of a past food web including Neandertal man. Journal of Human Evolution 20, 481-492.

Bookstein, F.L., 1997. Landmark methods for forms without landmarks: morphometrics of group differences in outline shape. Medical Image Analysis 1, 225-243.

Formatted: French (France)

Formatted: French (France)

Formatted: English (United States)

795 Brettell, R., Montgomery, J., Evans, J., 2012. Brewing and stewing: the effect of culturally mediated
796 behaviour on the oxygen isotope composition of ingested fluids and the implications for human
797 provenance studies. J. Anal. At. Spectrom. 27, 778-785.
798 Britton, K., Fuller, B.T., Tütken, T., Mays, S., Richards, M.P., 2015. Oxygen isotope analysis of human
799 bone phosphate evidences weaning age in archaeological populations. American Journal of Physical
800 Anthropology 157, 226-241.
801 Buzon, M.R., Bowen, G.J., 2010. Oxygen and carbon isotope analysis of human tooth enamel from the
802 New Kingdom site of Tombos in Nubia. Archaeometry 52, 855-868.
803 Buzon, M.R., Schrader, S.A., Bowen, G.J., 2019. Isotopic approaches to mobility in northern Africa: a
804 bioarchaeological examination of Egyptian/Nubian interaction in the Nile Valley, in: Mattingly, D.J.,
805 Sterry, M., Gatto, M.C., Ray, N. (Eds.), Burials, Migration and Identity in the Ancient Sahara and Beyond.
806 Cambridge University Press, Cambridge, pp. 223-246.
807 Buzon, M.R., Simonetti, A., 2013. Strontium isotope ($^{87}Sr/^{86}Sr$) variability in the Nile Valley: Identifying
808 residential mobility during ancient Egyptian and Nubian sociopolitical changes in the New Kingdom
809 and Napatan periods. American Journal of Physical Anthropology, 151, 1-9.
810 Buzon, M.R., Smith, S.T., Simonetti, A., 2016. Entanglement and the formation of the ancient Nubian
811 Napatan state. American Anthropologist 118, 284-300.
812 Castex, D., Blanchard, A., 2011. Témoignages archéologiques de crise(s) épidémique(s) : la catacombe
813 des Saints Marcellin et Pierre (Rome, fin I^{er}-III^{e} s.), in: Castex, D., Courtaud, P., Duday, H., Le Mort, F.,
814 Tillier, A.-M. (Eds.), Le regroupement des morts. Genèse et diversité archéologique. Editions Ausonius
815 - Maison des Sciences de l'Homme d'Aquitaine, Bordeaux, pp. 281-293.
816 Castex, D., Blanchard, A., Giuliani, R., Ricciardi, M., 2007. Les ensembles funéraires du secteur central
817 de la catacombe des Saints Pierre et Marcellin (Rome, I^{er}-III^{e} siècle) : caractérisation, hypothèses
818 d'interprétations et perspectives de recherches. Mélanges de l'École française de Rome - Antiquité
819 119, 274-282.
820 Castex, D., Blanchard, A., Réveillas, H., Kacki, S., Giuliani, R., 2009. Les sépultures du secteur central de
821 la catacombe des Saints Pierre-et-Marcellin (Rome). Etat des analyses bio-archéologiques et
822 perspectives Mélanges de l'Ecole française de Rome - Antiquité 121, 287-297.
823 Castex, D., Blanchard, P., Kacki, S., Réveillas, H., Giuliani, R., 2011. Le secteur central de la catacombe
824 des Sts Pierre-et-Marcellin (Rome, Ier-IIIe siècle). Indices archéologiques d'une crise brutale de
825 mortalité. Mélanges de l'Ecole Française de Rome – Chronique 123, 274-280.
826 Castex, D., Kacki, S., Reveillas, H., Souquet-Leroy, I., Sachau-Carcel, G., Blaizot, F.R., Blanchard, P.,
827 Duday, H., 2014. Revealing archaeological features linked to mortality increases. Anthropologie 52,
828 299-318.

829 Chenery, C.A., Pashley, V., Lamb, A.L., Sloane, H.J., Evans, J.A., 2012. The oxygen isotope relationship
830 between the phosphate and structural carbonate fractions of human bioapatite. Rapid
831 communications in mass spectrometry 26, 309-319.
832 Chisholm, B.S., Nelson, D.E., Schwarcz, H.P., 1982. Stable carbon isotope ratios as a measure of marine
833 versus terrestrial protein in ancient diets. Science 216, 1131-1132.
834 Collyer, M.L., Adams, D.C., 2018. An R package for fitting linear models to high-dimensional data using
835 residual randomization, Methods in Ecology and Evolution 9, 1772-1779.
836 Coplen, T.B., 1988. Normalization of oxygen and hydrogen isotope data. Chemical Geology: Isotope
837 Geoscience section 72, 293-297.
838 Craig, O.E., Biazzo, M., Colonese, A.C., di Giuseppe, Z., Martinez-Labarga, C., lo Vetro, D., Lelli, R.,
839 Martini, F., Rickards, O., 2010. Stable isotope analysis of Late Upper Palaeolithic human and faunal
840 remains from Grotta del Romito (Cosenza), Italy. Journal of Archaeological Science 37, 2504-2512.
841 Daux, V., Lécuyer, C., Héran, M.A., Amiot, R., Simon, L., Fourel, F., Martineau, F., Lynnerup, N., Reychler,
842 H., Escarguel, G., 2008. Oxygen isotope fractionation between human phosphate and water revisited.
843 Journal of Human Evolution 55, 1138-1147.
844 de Ligt, L., Tacoma, L.E., 2016. Migration and mobility in the Early Roman Empire. Brill, Leiden.
845 De Muynck, D., Huelga-Suarez, G., Van Heghe, L., Degryse, P., Vanhaecke, F., 2009. Systematic
846 evaluation of a strontium-specific extraction chromatographic resin for obtaining a purified Sr fraction
847 with quantitative recovery from complex and Ca-rich matrices. J. Anal. At. Spectrom. 24, 1498-1510.
848 DeNiro, M.J., 1985. Postmortem preservation and alteration of in vivo bone collagen ratios in relation
849 to palaeodietary reconstruction. Nature 317, 806-809.
850 Devièse, T., Ribechini, E., Castex, D., Stuart, B., Regert, M., Colombini, M.P., 2017. A multi-analytical
851 approach using FTIR, GC/MS and Py-GC/MS revealed early evidence of embalming practices in Roman
852 catacombs. Microchemical Journal 133, 49-59.
853 di Lernia, S., Tafuri, M.A., Gallinaro, M., Alhaique, F., Balasse, M., Cavorsi, L., Fullagar, P.D., Mercuri,
854 A.M., Monaco, A., Perego, A., Zerboni, A., 2013. Inside the "African Cattle Complex": Animal Burials in
855 the Holocene Central Sahara. PLOS ONE 8, e56879.
856 Dobberstein, R.C., Collins, M.J., Craig, O.E., Taylor, G., Penkman, K.E.H., Ritz-Timme, S., 2009.
857 Archaeological collagen: why worry about collagen diagenesis? Archaeological and Anthropological
858 Sciences 1, 31-42.
859 Drucker, D., Henry-Gambier, D., Lenoir, M., 2005. Alimentation humaine au cours du Magdalénien en
860 Gironde d'après les teneurs en isotopes stables (^{13}C, ^{15}N) du collagène. Paléo 17, 57-72.
861 Dupras, T.L., Schwarcz, H.P., Fairgrieve, S.I., 2001. Infant feeding and weaning practices in Roman
862 Egypt. American Journal of Physical Anthropology 115, 204-212.

Formatted: French (France)

Dufour, E., Van Neer, W., Vermeersch, P.M., Patterson, W.P., 2018. Hydroclimatic conditions and fishing practices at Late Paleolithic Makhadma 4 (Egypt) inferred from stable isotope analysis of otoliths. Quat. Int. 471, 190-202.

FAO, 1989. Yield and nutritional value of the commercially more important fish species. Food and agriculture organization of the United Nations, Rome.

Farah, E.A., Mustafa, E.M.A., Kumai, H., 2000. Sources of groundwater recharge at the confluence of the Niles, Sudan. Environmental Geology 39, 667-672.

Fernandes, R., Nadeau, M.J., Grootes, P.M., 2012. Macronutrient-based model for dietary carbon routing in bone collagen and bioapatite. Archaeological and Anthropological Sciences 4, 291-301.

Fernandes, R., Millard, A.R., Brabec, M., Nadeau, M.-J., Grootes, P., 2014. Food Reconstruction Using Isotopic Transferred Signals (FRUITS): a bayesian model for diet reconstruction. PLoS ONE 9, e87436.

Fiocchi Nicolai, V., Bisconti, F., Mazzoleni, D., 1999. The Christian Catacombs of Rome: History, Decoration, Inscriptions. Schnell und Steiner, Regensburg.

Garnsey, P., Saller, R.P., 1987. The Roman Empire: economy, society, and culture. University of California Press, Berkeley.

Garvie-Lok, S.J., 2001. Loaves and fishes: a stable isotope reconstruction of diet in medieval Greece. University of Calgary, Calgary, p. 525.

George, M., 2003. Images of Black slaves in the Roman empire. Syllecta Classica 14, 161-185.

Giuliani, R., Castex, D., Blanchard, P., Coquerelle, M., 2007. La scoperta di un nuovo santuario nella catacomba dei SS. Marcellino e Pietro e lo scavo antropologico degli insiemi funerari annessi. Risultati preliminari di un'indagine multidisciplinare. Rendiconti della Pontificia Accademia Romana di Archeologia 79, 83-124.

Gleize, Y., Mendisco, F., Pemonge, M.-H., Hubert, C., Groppi, A., Houix, B., Deguilloux, M.-F., Breuil, J.-Y., 2016. Early medieval Muslim graves in France: First archaeological, anthropological and palaeogenomic evidence. PLOS ONE 11, e0148583.

Gordon, M.L., 1924. The nationality of slaves under the early Roman empire. The Journal of Roman Studies 14, 93-111.

Gower, J.C., 1971. A general coefficient of similarity and some of its properties. Biometrics 27, 857-871.

Hedges, R.E.M., Reynard, L.M., 2007. Nitrogen isotopes and the trophic level of humans in archaeology. Journal of Archaeological Science 34, 1240-1251.

Heinz, G., Heutzinger, P., 2007. Meat processing technology for small- to medium-scale producers. Food and Agriculture Organization of the United Nations, Bangkok.

Herring, D.A., Saunders, S.R., Katzenberg, M.A., 1998. Investigating the weaning process in past populations. American Journal of Physical Anthropology 105, 425-439.

Formatted: English (United States)

Formatted: English (United States)

898 Hilgers, W., 1969. Lateinische gefässnamen. Rheinland-Verlag, Düsseldorf.
899 Howland, M.R., Corr, L.T., Young, S.M., Jones, V., Jim, S., van der Merwe, N.J., Mitchell, A.D., Evershed,
900 R.P., 2003. Expression of the dietary isotope signal in the compound-specific $\delta^{13}C$ values of pig bone
901 lipids and amino acids. International Journal of Osteoarchaeology 13, 54-65.
902 Iacumin, P., Bocherens, H., Chaix, L., 2001. Keratin C and N stable isotope ratios of fossil cattle horn
903 from Kerma (Sudan): a record of dietary changes. Quaternario 14, 41-46.
904 Iacumin, P., Bocherens, H., Chaix, L., Marioth, A., 1998. Stable carbon and nitrogen isotopes as dietary
905 indicators of ancient Nubian populations (Northern Sudan). Journal of Anthropological Archaeology
906 25, 293-301.
907 Iacumin, P., Bocherens, H., Mariotti, A., Longinelli, A., 1996. An isotopic palaeoenvironmental study of
908 human skeletal remains from the Nile Valley Palaeogeography, Palaeoclimatology, Palaeoecology 126,
909 15-30.
910 Iacumin, P., Di Matteo, A., Usai, D., Salvatori, S., Venturelli, G., 2016. Stable isotope study on ancient
911 populations of central Sudan: Insights on their diet and environment. American Journal of Physical
912 Anthropology 160, 498-518.
913 Irish, J.D., 2005. Population continuity vs. discontinuity revisited: Dental affinities among Late
914 Paleolithic through Christian-era Nubians. American Journal of Physical Anthropology 128, 520-535.
915 Kacki, S., Réveillas, H., Sachau-Carcel, G., Giuliani, R., Blanchard, P., Castex, D., 2014. Réévaluation des
916 arguments de simultanéité des dépôts de cadavres: l'exemple des sépultures plurielles de la
917 catacombe des Saints Pierre-et-Marcellin (Rome). Bulletins et mémoires de la Société d'anthropologie
918 de Paris, 1-10.
919 Keenleyside, A., Schwarcz, H.P., Stirling, L., Ben Lazreg, N., 2009. Stable isotopic evidence for diet in a
920 Roman and Late Roman population from Leptiminus, Tunisia. Journal of Archaeological Science 36, 51-
921 63.
922 Kendall, D.G., 1984. Shape manifolds, procrustean metrics, and complex projective spaces. Bulletin of
923 the London Mathematical Society 16, 81-121.
924 Kennedy, G.E., 2005. From the ape's dilemma to the weanling's dilemma: early weaning and its
925 evolutionary context. Journal of Human Evolution 48, 123-145.
926 Killgrove, K., Tykot, R.H., 2013. Food for Rome: a stable isotope investigation of diet in the Imperial
927 period (1st–3rd centuries AD). Journal of Anthropological Archaeology 32, 28-38.
928 Killgrove, K., Montgomery, J., 2016. All Roads Lead to Rome: Exploring Human Migration to the Eternal
929 City through Biochemistry of Skeletons from Two Imperial-Era Cemeteries (1st-3rd c AD). PLOS ONE
930 11, e0147585.
931 Killgrove, K., Tykot, R.H., 2018. Diet and collapse: A stable isotope study of Imperial-era Gabii (1st–3rd
932 centuries AD). Journal of Archaeological Science: Reports 19, 1041-1049.

933 Kirwan, L.P., 1957. Rome beyond the southern Egyptian frontier. The Geographical Journal 123, 13-19.
934 Knudson, K.J., 2009. Oxygen isotope analysis in a land of environmental extremes: the complexities of
935 isotopic work in the Andes. International Journal of Osteoarchaeology 19, 171-191.
936 Koch, P.L., Tuross, N., Fogel, M.L., 1997. The effects of sample treatment and diagenesis on the isotopic
937 integrity of carbonate in biogenic hydroxylapatite. Journal of Archaeological Science 24, 417-429.
938 La Piana, G., 1927. Foreign groups in Rome during the first centuries of the Empire. Harvard Theological
939 Review 20, 183-403.
940 Law, R.C.C., 2009. The Garamantes and trans-Saharan enterprise in Classical times. The Journal of
941 African History 8, 181-200.
942 Lebon, M., Muller, K., Bahain, J.-J., Frohlich, F., Falgueres, C., Bertrand, L., Sandt, C., Reiche, I., 2011.
943 Imaging fossil bone alterations at the microscale by SR-FTIR microspectroscopy. J. Anal. At. Spectrom.
944 26, 922-929.
945 Lenski, N., 2006. *Servi Publici* in Late Antiquity, in: Krause, J.-U., Witschel, C. (Eds.), Die stadt in der
946 spätantike - Niedergang oder wander? Verlag, Stuttgart, pp. 335-357.
947 Longin, R., 1971. New method of collagen extraction for radiocarbon dating. Nature 230, 241-242.
948 Maaranen, N., Zakrzewski, S.R., Schutkowski, H., 2019. Hyksos in Egypt – utilising biodistance methods
949 to interpret archaeological and textual evidence from Tell el-Dab'a, American Journal of Physical
950 Anthropologists, 171, S69, 149.
951 Maechler, M., Rousseeuw, P., Struyf, A., Hubert, M., Hornik, K., 2019. cluster: Cluster Analysis Basics
952 and Extensions. R package version 2.1.0.
953 Marado, L.M., Silva, A.M., 2016. The mandibular molar pit-tubercle (MMPT) dental nonmetric trait:
954 Comprehensive analysis of a large sample. HOMO 67, 462-470.
955 Martiniano, R., Caffell, A., Holst, M., Hunter-Mann, K., Montgomery, J., Müldner, G., McLaughlin, R.L.,
956 Teasdale, M.D., van Rheenen, W., Veldink, J.H., van den Berg, L.H., Hardiman, O., Carroll, M., Roskams,
957 S., Oxley, J., Morgan, C., Thomas, M.G., Barnes, I., McDonnell, C., Collins, M.J., Bradley, D.G., 2016.
958 Genomic signals of migration and continuity in Britain before the Anglo-Saxons. Nature
959 Communications 7, 10326.
960 Marzano, A., 2018. Fish and Fishing in the Roman World. Journal of Maritime Archaeology 13, 437-447.
961 McArthur, J.M., 2001. Strontium isotope stratigraphy: LOWESS version 3: Best fit to the marine Sr-
962 isotope curve for 0–509 Ma and accompanying look-up table for deriving numerical age. Journal of
963 Geology 109, 155-170.
964 McLaughlin, R., 2014. The Roman empire and the Indian ocean. Pen & Sword, Barnsley.
965 Mitteroecker, P., Gunz, P., 2009. Advances in geometric morphometrics. Evolutionary Biology 36, 235-
966 247.

967 Moharrery, A., 2007. Effect of docking and energy of diet on carcass fat characteristics in fat-tailed
968 Badghisian sheep. Small Ruminant Research 69, 208-216.
969 Moorrees, C.F.A., Fanning, E.A., Hunt, E.E., 1963. Age variation of formation stages for ten permanent
970 teeth. Journal of Dental Research 42, 1490-1502.
971 Nehlich, O., Richards, M.P., 2009. Establishing collagen quality criteria for sulphur isotope analysis of
972 archaeological bone collagen. Archaeological and Anthropological Sciences 1, 59-75.
973 Nehlich, O., 2015. The application of sulphur isotope analyses in archaeological research: a review.
974 Earth-Science Reviews 142, 1-17.
975 Nichol, C.R., 1990. Dental genetics and biological relationships of the Pima Indians of Arizona. Arizona
976 State University, Tempe.
977 Nitsch, E.K., 2012. Stable isotope evidence for diet change in Roman and Medieval Italy: local, regional
978 and continental perspectives, School of Archaeology. University of Oxford, Oxford, p. 352.
979 Noy, D., 2000. Foreigners at Rome: citizens and strangers. Duckworth, London.
980 O'Connell, T.C., Ballantyne, R.M., Hamilton-Dyer, S., Margaritis, E., Oxford, S., Pantano, W., Millett, M.,
981 Keay, S.J., 2019. Living and dying at the Portus Romae. Antiquity 93, 719-734.
982 Olsen, A.M., Westneat, M.W., 2015. StereoMorph: an R package for the collection of 3D landmarks
983 and curves using a stereo camera set-up, Methods in Ecology and Evolution, 351-356.
984 Passey, B.H., Robinson, T.F., Ayliffe, L.K., Cerling, T.E., Sponheimer, M., Dearing, M.D., Roeder, B.L.,
985 Ehleringer, J.R., 2005. Carbon isotope fractionation between diet, breath CO_2, and bioapatite in
986 different mammals. Journal of Archaeological Science 32, 1459-1470.
987 Peterson, B.J., Howarth, R.W., Garritt, R.H., 1985. Multiple stable isotopes used to trace the flow of
988 organic matter in estuarine food webs. Science 227, 1361-1363.
989 Pilloud, M.A., Maier, C., Scott, G.R., Edgar, H.J.H., 2018. Molar crenulation trait definition and variation
990 in modern human populations. HOMO 69, 77-85.
991 Prowse, T.L., 2001. Isotopic and dental evidence for diet from the necropolis of Isola Sacra (1st-3rd
992 centuries AD), Italy, Department of Anthropology. McMaster University, Hamilton, p. 356.
993 Prowse, T., Schwarcz, H.P., Saunders, S., Macchiarelli, R., Bondioli, L., 2004. Isotopic paleodiet studies
994 of skeletons from the Imperial Roman-age cemetery of Isola Sacra, Rome, Italy. Journal of
995 Archaeological Science 31, 259-272.
996 Prowse, T.L., Saunders, S.R., Schwarcz, H.P., Garnsey, P., Macchiarelli, R., Bondioli, L., 2008. Isotopic
997 and dental evidence for infant and young child feeding practices in an Imperial Roman skeletal sample.
998 American Journal of Physical Anthropology 137, 294-308.
999 Purcell, N., 1995. Eating fish: the paradoxes of seafood, in: Wilkins, J., Harvey, D., Dobson, M. (Eds.),
1000 Food in Antiquity. University of Exeter Press, Exeter, pp. 132-149.

Reitsema, L.J., 2012. Stable carbon and nitrogen isotope analysis of human diet change in prehistoric and historic Poland, Department of Anthropology. The Ohio State University, Columbus, p. 377.

Rhine, S., 1990. Non-metric skull racing, in: Gill, G.W., Rhine, S. (Eds.), Skeletal attribution of race. Maxwell Museum of Anthropology, Albuquerque, pp. 9–20.

Richards, M.P., Karavanić, I., Pettitt, P., Miracle, P., 2015. Isotope and faunal evidence for high levels of freshwater fish consumption by Late Glacial humans at the Late Upper Palaeolithic site of Šandalja II, Istria, Croatia. Journal of Archaeological Science 61, 204-212.

Rivollat, M., Mendisco, F., Pemonge, M.-H., Safi, A., Saint-Marc, D., Brémond, A., Couture-Veschambre, C., Rottier, S., Deguilloux, M.-F., 2015. When the waves of European Neolithization met: First paleogenetic evidence from early farmers in the southern Paris Basin. PLOS ONE 10, e0125521.

Roberts, S.B., Coward, W.A., Ewing, G., Savage, J., Cole, T.J., Lucas, A., 1988. Effect of weaning on accuracy of doubly labeled water method in infants. American Journal of Physiology - Regulatory, Integrative and Comparative Physiology 254, R622-R627.

Royer, A., Daux, V., Fourel, F., Lécuyer, C., 2017. Carbon, nitrogen and oxygen isotope fractionation during food cooking: Implications for the interpretation of the fossil human record. American Journal of Physical Anthropology 163, 759-771.

Rutgers, L.V., van Strydonck, M., Boudin, M., van der Linde, C., 2009. Stable isotope data from the early Christian catacombs of ancient Rome: new insights into the dietary habits of Rome's early Christians. Journal of Archaeological Science 36, 1127–1134.

Salesse, K., 2015. Archéo-biogéochimie isotopique, reconstitutions des régimes alimentaires et des schémas de mobilité, et interactions bio-culturelles. Les sépultures plurielles de la région X de la catacombe des Saints Pierre-et-Marcellin (Rome, I^{er}-III^{e} s. ap. J.-C.). Université de Bordeaux, Bordeaux, p. 352.

Salesse, K., Dufour, E., Lebon, M., Wurster, C., Castex, D., Bruzek, J., Zazzo, A., 2014. Variability of bone preservation in a confined environment: the case of the catacomb of Sts Peter and Marcellinus (Rome, Italy). Palaeogeography, Palaeoclimatology, Palaeoecology 416, 43-54.

Salesse, K., Fernandes, R., de Rochefort, X., Brůžek, J., Castex, D., Dufour, É., 2018. IsoArcH.eu: an open-access and collaborative isotope database for bioarchaeological samples from the Graeco-Roman world and its margins. Journal of Archaeological Science: Reports 19, 1050-1055.

Salesse, K., Fernandes, R., de Rochefort, X., Brůžek, J., Castex, D., Dufour, É., 2020. www.IsoArcH.eu (v.1.1). accessed 26/04/2020.

Schirmer, C., 2014. Food and status in ancient Rome: the evidence from literature. Pithos 13, 1-20.

Schoeninger, M.J., DeNiro, M.J., Tauber, H., 1983. Stable nitrogen isotope ratios of bone collagen reflect marine and terrestrial components of Prehistoric human diet. Science 220, 1381-1383.

Formatted: English (United States)

1035 Schotsmans, E.M.J., Toksoy-Köksal, F., Brettell, R.C., Bessou, M., Corbineau, R., Lingle, A.M., Bouquin,
1036 D., Blanchard, P., Becker, K., Castex, D., Knüsel, C.J., Wilson, A.S., Chapoulie, R., 2019. 'Not All That Is
1037 White Is Lime'—White Substances from Archaeological Burial Contexts: Analyses and Interpretations.
1038 Archaeometry 61, 809-827.
1039 Schrader, S.A., Buzon, M.R., Corcoran, L., Simonetti, A., 2019. Intraregional $^{87}Sr/^{86}Sr$ variation in Nubia:
1040 New insights from the Third Cataract. Journal of Archaeological Science: Reports 24, 373-379.
1041 Scott, G.R., Irish, J.D., 2017. Human tooth crown and root morphology: The Arizona State University
1042 dental anthropology system. Cambridge University Press, Cambridge.
1043 Sellen, D.W., 2001. Comparison of infant feeding patterns reported for nonindustrial populations with
1044 current recommendations. The Journal of Nutrition 131, 2707-2715.
1045 Sellen, D.W., 2007. Evolution of infant and young child feeding: implications for contemporary public
1046 health. Annual Review of Nutrition 27, 123-148.
1047 Sereno, P.C., Garcea, E.A.A., Jousse, H., Stojanowski, C.M., Saliège, J.-F., Maga, A., Ide, O.A., Knudson,
1048 K.J., Mercuri, A.M., Stafford, T.W., Jr., Kaye, T.G., Giraudi, C., N'Siala, I.M., Cocca, E., Moots, H.M.,
1049 Dutheil, D.B., Stivers, J.P., 2008. Lakeside cemeteries in the Sahara: 5000 Years of Holocene population
1050 and environmental change. PLOS ONE 3, e2995.
1051 Silver, M., 2016. Public slave in the Roman army: an exploratory study. Ancient Society 46, 203-240.
1052 Snowden Jr., F.M., 1947. The Negro in Classical Italy. The American Journal of Philology 68, 266-292.
1053 Spangenberg, J.E., Vennemann, T.W., 2008. The stable hydrogen and oxygen isotope variation of water
1054 stored in polyethylene terephthalate (PET) bottles. Rapid communications in mass spectrometry 22,
1055 672-676.
1056 Spurr, M.S., 1983. The cultivation of millet in Roman Italy. Papers of the British School at Rome 51, 1-
1057 15.
1058 Stojanowski, C.M., Knudson, K.J., 2011. Biogeochemical inferences of mobility of early Holocene fisher-
1059 foragers from the Southern Sahara Desert. American Journal of Physical Anthropology 146, 49-61.
1060 Stojanowski, C.M., Knudson, K.J., 2014. Changing patterns of mobility as a response to climatic
1061 deterioration and aridification in the middle Holocene southern Sahara. American Journal of Physical
1062 Anthropology 154, 79-93.
1063 Tacoma, L.E., 2012. Number games. Quantifying immigrants in Rome, Moving Romans conference,
1064 Leiden, pp. 1-30.
1065 Tacoma, L.E., 2016. Moving Romans : migration to Rome in the principate. Oxford University Press,
1066 Oxford.
1067 Tafuri, M.A., Bentley, R.A., Manzi, G., di Lernia, S., 2006. Mobility and kinship in the prehistoric Sahara:
1068 Strontium isotope analysis of Holocene human skeletons from the Acacus Mts. (southwestern Libya).
1069 Journal of Anthropological Archaeology 25, 390-402.

Tafuri, M.A., Goude, G., Manzi, G., 2018. Isotopic evidence of diet variation at the transition between classical and post-classical times in Central Italy. Journal of Archaeological Science: Reports 21, 496-503.

Team, R.C., 2020. R: A language and environment for statistical computing, URL https://www.R-project.org/.

Thompson, A.H., Chaix, L., Richards, M.P., 2008. Stable isotopes and diet at Ancient Kerma, Upper Nubia (Sudan). Journal of Archaeological Science 35, 376-387.

Touzeau, A., Blichert-Toft, J., Amiot, R., Fourel, F., Martineau, F., Cockitt, J., Hall, K., Flandrois, J.-P., Lécuyer, C., 2013. Egyptian mummies record increasing aridity in the Nile valley from 5500 to 1500 yr before present. Earth and Planetary Science Letters 375, 92-100.

Tsutaya, T., Yoneda, M., Abe, M., Nagaoka, T., 2019. Carbon, nitrogen, and sulfur stable isotopic reconstruction of human diet in a mountainous woodland village in Sendaiji in premodern Japan. Anthropological Science 127, 131-138.

Turchi, C., Buscemi, L., Previderè, C., Grignani, P., Brandstätter, A., Achilli, A., Parson, W., Tagliabracci, A., Group, G.F.I., 2008. Italian mitochondrial DNA database: results of a collaborative exercise and proficiency testing. International Journal of Legal Medicine 122, 199-204.

van der Maaten, L., Hinton, G., 2008. Visualizing data using t-SNE. Journal of Machine Learning Research 9, 2579-2605.

Van Klinken, G.J., 1999. Bone collagen quality indicators for palaeodietary and radiocarbon measurements. Journal of Archaeological Science 26, 687-695.

Wang, Y., Cerling, T.E., 1994. A model of fossil tooth and bone diagenesis: implications for paleodiet reconstruction from stable isotopes. Palaeogeography, Palaeoclimatology, Palaeoecology 107, 281-289.

Warinner, C., Tuross, N., 2009. Alkaline cooking and stable isotope tissue-diet spacing in swine: archaeological implications. Journal of Archaeological Science 36, 1690-1697.

Webster, M., Sheets, H.D., 2010. A Practical Introduction to landmark-based geometric morphometrics. The Paleontological Society Papers 16, 163-188.

Weiss, A., 2004. Sklave der Stadt: Untersuchungen zur öffentlichen Sklaverei in den Städten des Römischen Reiches. Verlag, Stuttgart.

Wilson, A., 2012. Saharan trade in the Roman period: short-, mediumand long-distance trade networks. Azania: Archaeological Research in Africa 47, 409-449.

Wright, L.E., Schwarcz, H.P., 1998. Stable carbon and oxygen isotopes in human tooth enamel: identifying breastfeeding and weaning in Prehistory. American Journal of Physical Anthropology 106, 1-18.

Wright, L.E., Schwarcz, H.P., 1999. Correspondence between stable carbon, oxygen and nitrogen isotopes in human tooth enamel and dentine: infant diets at Kaminaljuyú. Journal of Archaeological Science 26, 1159-1170.

Zazzo, A., 2014. Bone and enamel carbonate diagenesis: a radiocarbon prospective. Palaeogeography, Palaeoclimatology, Palaeoecology 416, 168-178.